Available online at www.sciencedirect.com
ScienceDirect
Polymer 48 (2007) 5960–5978
polymer
www.elsevier.com/locate/polymer

Effect of the ratio of maleated polypropylene to organoclay on the structure and properties of TPO-based nanocomposites. Part I: Morphology and mechanical properties

Do Hoon Kim [a], Paula D. Fasulo [b], William R. Rodgers [b], D.R. Paul [a,*]

[a] *Department of Chemical Engineering and Texas Materials Institute, The University of Texas at Austin, Austin, TX 78712-1062, United States*
[b] *General Motors Research and Development Center, 30500 Mound Road, Warren, MI 48090, United States*

Received 16 May 2007; received in revised form 2 August 2007; accepted 3 August 2007
Available online 9 August 2007

Abstract

The structure–property relationships of thermoplastic olefin (TPO)-based nanocomposites prepared by melt processing are reported with a main focus on the ratio of maleic anhydride-grafted polypropylene (PP-*g*-MA) to organoclay. The morphological observations by transmission electron microscopy, atomic force microscopy, and X-ray diffraction are presented in conjunction with the mechanical and rheological properties of these nanocomposites. Detailed quantitative analyses of the dispersed clay particles revealed that the aspect ratio of clay particles decreased as clay content increased but increased as the amount of PP-*g*-MA increased. Analysis of the elastomer phase revealed that the aspect ratio of the elastomer phase increased in both cases. The presence of clay causes the elastomer particles to become highly elongated in shape and retards the coalescence of the elastomer particles. The modulus and yield strength are enhanced by increasing the PP-*g*-MA/organoclay ratios. High levels of toughness of the TPO can be maintained when moderate levels of (organoclay) MMT and PP-*g*-MA are used. The rheological properties suggested that the addition of clay particles and PP-*g*-MA has a profound influence on the long time stress relaxation of the TPO nanocomposites. Based on these analyses, it is clear that it is important to optimize the ratio of PP-*g*-MA and organoclay to obtain the desired balance of mechanical properties and processing characteristics for TPO nanocomposites.

Keywords: Polymer nanocomposites; Thermoplastic olefin (TPO); PP-*g*-MA

1. Introduction

There has been a continued interest in polymer/layered silicate nanocomposites since the first synthesis of nylon/clay nanocomposites via in situ polymerization [1–6]. Layered silicates can impart high levels of reinforcement to polymers at very low concentrations which makes them attractive for replacement of conventional fillers, e.g., talc or glass fibers, in many applications. The focus of most industrial research and development has been on the formation of nanocomposites by melt mixing or compounding processes because this is generally more commercially attractive than in situ polymerization [3,5].

Polyolefin/layered silicate nanocomposites, especially polypropylene (PP), have been widely investigated for replacement of high performance engineering thermoplastics with lower cost materials [7–21]. PP has great potential for nanocomposite applications because of many desirable properties, such as low density, high thermal stability, and good solvent resistance. However, its lower modulus relative to engineering polymers and brittle nature represent practical limitations for many applications. Inorganic fillers can increase stiffness, reduce mold shrinkage, and thermal expansion while an elastomer phase can be used to compensate for the reduction of toughness, particularly at low temperature,

* Corresponding author. Tel.: +1 512 471 5392; fax: +1 512 471 0542.
E-mail address: drp@che.utexas.edu (D.R. Paul).

0032-3861/$ - see front matter © 2007 Elsevier Ltd. All rights reserved.
doi:10.1016/j.polymer.2007.08.010

caused by adding filler. Thus, a major issue for some applications is to achieve an optimum balance of stiffness and toughness. To address this, elastomer toughened PP, or the so-called ''thermoplastic olefin'' or TPO, materials containing talc as a filler are widely used to produce automotive exterior and interior parts [22–25]. The morphology of the dispersed phases, both elastomer and filler, and processing conditions play an important role in determining the stiffness and toughness of PP/elastomer/filler composites [24–26]. However, due to the low aspect ratio of conventional fillers such as talc, large loadings are required to significantly increase stiffness, which can result in poor processability, lower ductility, and a rough surface finish. Replacing such fillers with high aspect ratio, nanometer thick layered silicates could potentially alleviate these issues, assuming that good levels of clay dispersion can be achieved.

Since non-polar PP does not inherently achieve a high level of dispersion of organoclays, it has been found useful to add small amounts of a maleated PP, or PP-*g*-MA, to serve as a ''compatibilizer'' to achieve better dispersion of the silicate platelets in the PP or TPO matrix and as a consequence, improved stiffness of PP or TPO nanocomposites. Even though there are some reports on the formation of PP/organoclay nanocomposites without any compatibilizer by chemical [8,27,28] and physical [29–31] methods, most commercial nanocomposites of this type contain PP-*g*-MA. Interestingly, very few studies have reported how the ratio of PP-*g*-MA to organoclay affects morphology and the performance of PP-based nanocomposites [12,17,32] or TPO-based nanocomposites [33,34]. Recently, Lee et al. described the phase morphology and the mechanical and thermal expansion behaviors of nanocomposites prepared from PP reinforced with an organoclay and toughened with an ethylene–octene elastomer using a masterbatch material containing equal parts of PP-*g*-MA and an organoclay [35,36]. We recently reported the effect of the PP-*g*-MA/organoclay ratio on the morphology and performance, e.g., mechanical, rheological, and thermal expansion behaviors, for PP-based nanocomposites that contained no elastomer phase [37].

The purpose of this study is to examine more fully how the ratio of PP-*g*-MA to organoclay affects the structure–property relationships of TPO-based nanocomposites. In this work, a reactor-made TPO is used; whereas, the prior work by Lee et al. [35,36] used an extruder-made melt blend of PP and elastomer. Generally, reactor-made TPOs have a better optimized elastomer particle size for toughness; however, use of such materials eliminates the ability to easily vary the elastomer/PP ratio in the compounded formulation. A detailed particle analysis for both filler and elastomer phases is presented here and is used to understand the mechanical and rheological properties of these nanocomposites. As expected, the mechanical and rheological properties of TPO nanocomposites depend strongly on the change in the morphology of the dispersed clay and elastomer particles as the PP-*g*-MA/organoclay ratio is varied. Subsequent papers will discuss the thermal expansion behavior and the modeling of stiffness and thermal expansion of these nanocomposites.

2. Experimental

2.1. Materials and composite preparation

Nanocomposites were formed by melt compounding mixtures of a commercial TPO (CA387 from Basell, melt index = 17 g/10 min), maleic anhydride-grafted polypropylene (Polybond 3200 from Chemtura, MA content = 1.0 wt%), and an organoclay (Cloisite 20A from Southern Clay Products). Compounding was carried out using a Haake co-rotating twin screw extruder (length = 305 mm, $L/D = 10$) set at a barrel temperature of 170 °C (feed), a die temperature of 190 °C, a screw speed of 280 rpm, and a feed rate of 1 kg/h. TPO nanocomposites were made with different ratios of PP-*g*-MA to organoclay at fixed MMT contents as depicted in Fig. 1. Based on comparisons with physical blends of PP and ethylene/octane copolymer from prior studies [35,36], it appears that this commercial TPO contains about 25% by weight of elastomer.

Extruded nanocomposite pellets were dried and then injection molded into standard tensile (ASTM D638, Type I) and Izod (ASTM D256) bars in an Arburg Allrounder 305-210-700 injection molding machine using a barrel temperature of 180 °C (feed) to 220 °C (die), mold temperature of 40 °C, injection pressure of 35 bar, and a holding pressure of 35 bar. The amount of montmorillonite (MMT) in each extruded batch was determined by placing the central portion of a tensile or Izod bar (~3 g each) in a furnace at 900 °C for 45 min and weighing the remaining MMT ash with appropriate correction for loss of structural water during incineration [38,39]. The numbers inside the circles in Fig. 1 indicate the actual MMT content of each nanocomposite.

2.2. Morphological characterization and particle analysis for the filler and elastomer

Samples for transmission electron microscopic (TEM) analysis were taken from the central and skin regions of an

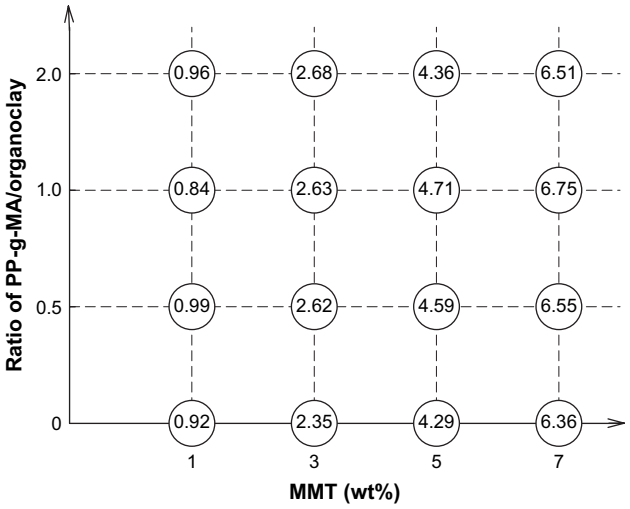

Fig. 1. Experimental plan for examining the effects of PP-*g*-MA and organoclay contents. The numbers inside the circles are the actual amount of montmorillonite (wt%) in the TPO-based nanocomposites as determined by burning off the polymer in a furnace.

Izod bar. The central sample regions were located parallel and perpendicular to the flow direction ca. 3–4 cm away from the far end of a 13 cm Izod bar and halfway between the top and the bottom surfaces of the bar. Sections taken from the core region of injection-molded specimens were viewed in the three orthogonal directions, flow direction (FD), transverse direction (TD), and normal direction (ND). Schematic illustrations of this nomenclature can be found elsewhere [35,36,40,41]. TEM analyses were made on a view observed parallel to the transverse direction (TD), or in the FD–ND plane, in this paper. The morphologies viewed parallel to the flow direction (FD), or in the TD–ND plane, and viewed parallel to the normal direction (ND), or in the FD–TD plane, will be presented in subsequent papers. Ultra-thin sections ranging from 50 to 70 nm in thickness were cryogenically cut with a diamond knife at temperatures of −65 °C for the specimen and −58 °C for the knife using an RMC PowerTome XL ultramicrotome with a CR-X universal cryo-sectioning system. Sections were collected on 300 mesh copper TEM grids and subsequently dried with filter paper. The sections were examined by TEM using a JEOL 2010F TEM with a LaB_6 filament operating at an accelerating voltage of 120 kV.

Atomic force microscopic (AFM) experiments were performed on cryogenically microtomed surfaces of nanocomposites containing elastomer using a Digital Instruments Dimension 3100 with Nanoscope IV controller at room temperature. Images were recorded in the tapping mode using etched silicon probes. The instrumental parameters such as the set point and the gain were adjusted to improve the image resolution.

Wide angle X-ray scattering (WAXS) scans were made using a Scintag XDS 2000 diffractometer in the reflection mode using an incident X-ray wavelength of 1.542 Å at a scan rate of 1.0°/min over the range of $2\theta = 1°–30°$. X-ray analyses were performed at room temperature on as-molded specimens. The Izod specimens were oriented such that the incident beam reflected off the transverse face.

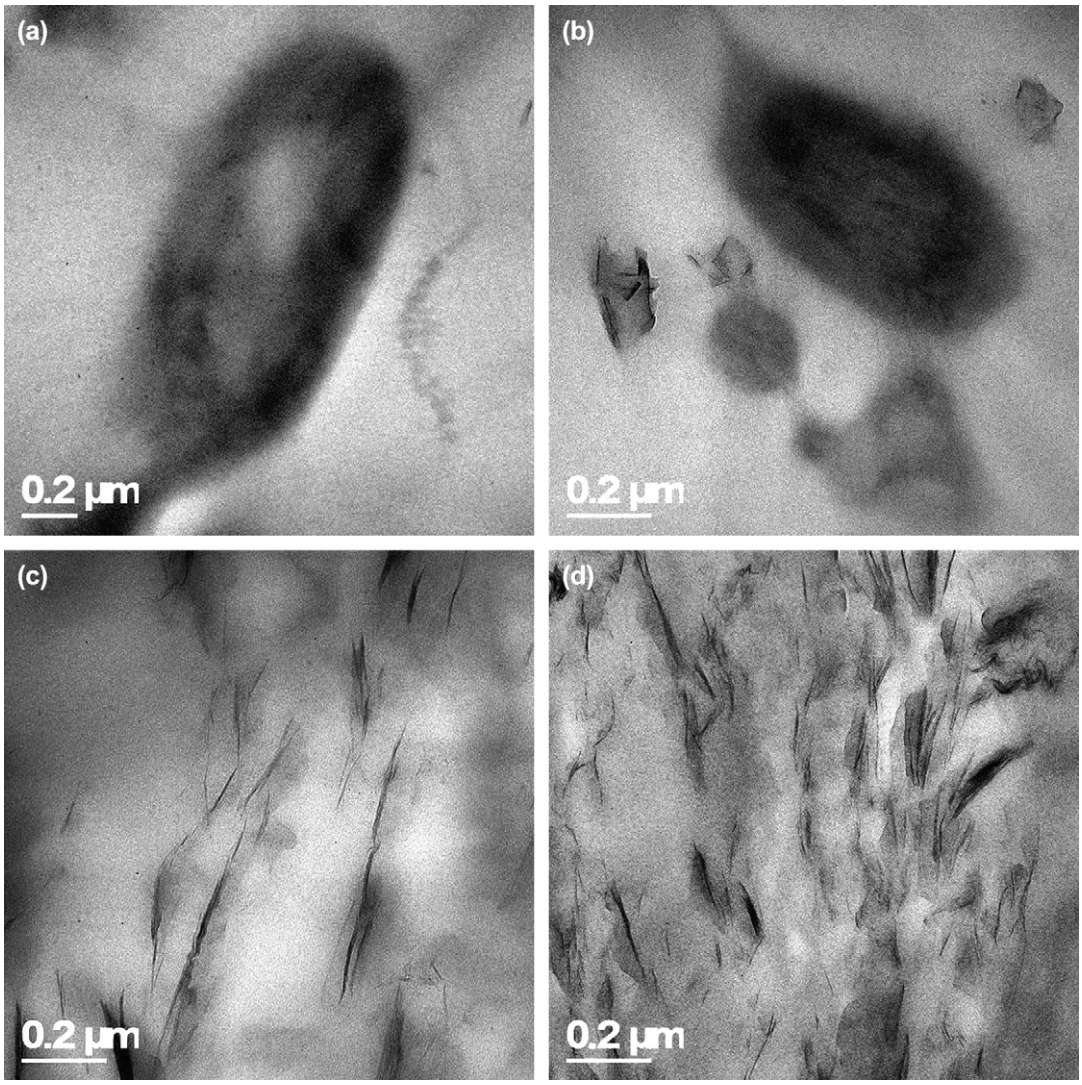

Fig. 2. TEM micrographs of TPO/PP-*g*-MA/MMT nanocomposites showing clay and rubber particle morphology for MMT contents of (a) 0, (b) 1, (c) 3, and (d) 7 wt% at a fixed ratio of PP-*g*-MA to organoclay of 1.0. Images were taken from the core of the sample and viewed parallel to the TD.

2.3. Mechanical properties

Stress–strain analyses were performed according to ASTM D638 using an Instron model 1137 upgraded for computerized data acquisition. Specimen modulus was determined using an extensometer at a crosshead speed of 0.51 cm/min, while yield strength was determined at a speed of 5.1 cm/min. Tensile property values reported here represent an average from measurements on at least five specimens.

Notched Izod impact tests were performed at room temperature using a TMI Izod tester (6.8 J hammer and 3.5 m/s impact velocity) according to ASTM D256. Property values reported here represent an average from, at least, five specimens.

2.4. Rheological properties

A Rheometrics Mechanical Spectrometer (RMS 800) was used to determine the rheological performance of the TPO-based nanocomposites, using the parallel fixture. All the rheological measurements were carried out at a fixed temperature of 180 °C under a nitrogen gas flow. Strain sweep tests were carried out for each sample to ensure that the strain used is within the linear viscoelastic range. Frequency sweep tests were made over a frequency range of 0.1–200 rad/s at strain of 1–5%, which is within the linear region for each sample. Specimens for rheological testing were molded in a hot press (Carver, CH 4386) at 180 °C for 5 min. The molded samples were of disc shape with a diameter of 25 mm and 1 mm thickness.

3. Results and discussion

3.1. Morphological characterization using TEM and AFM

The degree of dispersion or exfoliation of the layered silicate plays an important role in the performance, e.g., mechanical and thermal expansion, etc., of polymer nanocomposites.

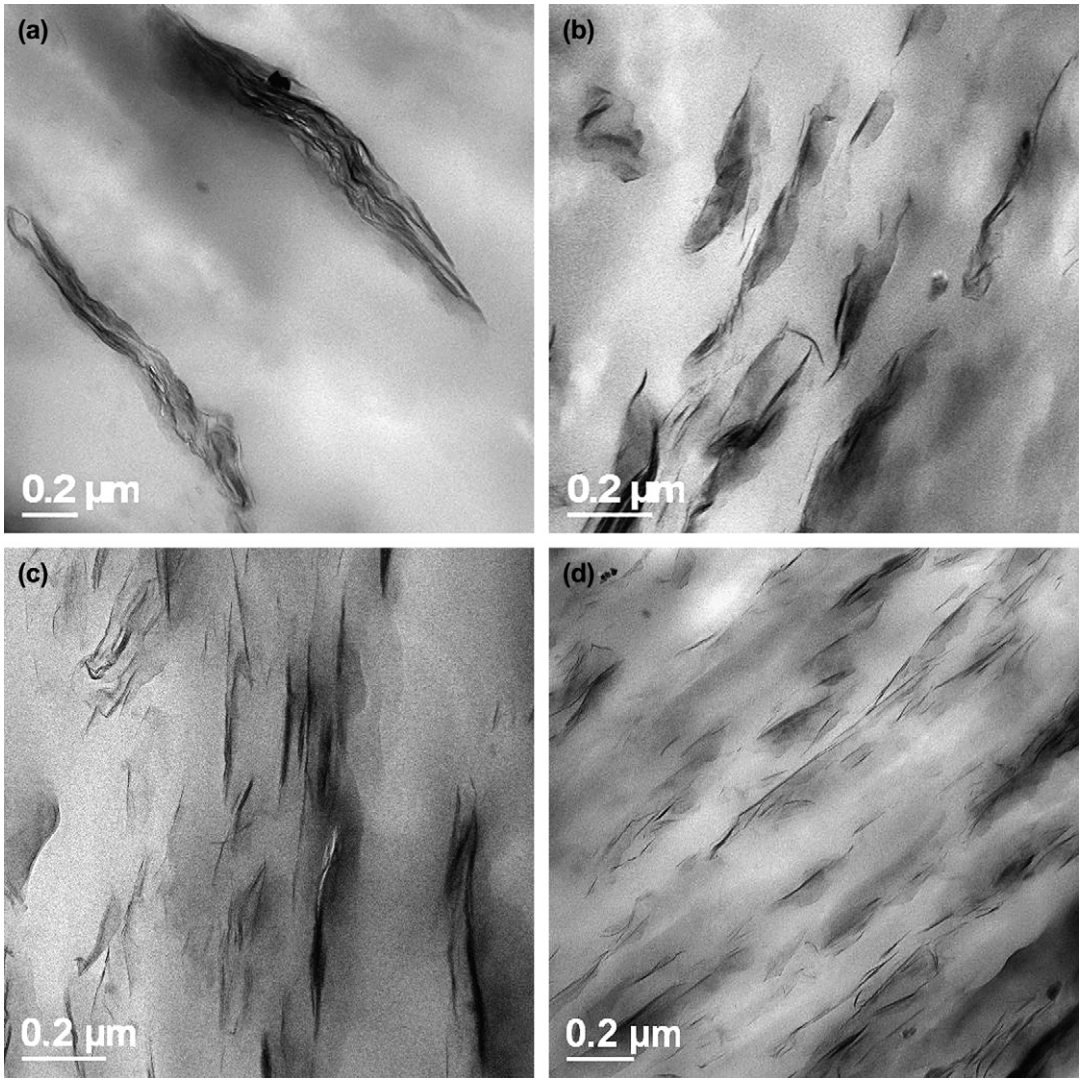

Fig. 3. TEM micrographs of TPO/PP-*g*-MA/MMT nanocomposites showing clay and rubber particle morphology for PP-*g*-MA to organoclay ratios of (a) 0, (b) 0.5, (c) 1.0, and (d) 2.0 at a fixed MMT of 5 wt%. Images were taken from the core of the sample and viewed parallel to the TD.

While well-exfoliated clay platelets can be dispersed through the matrix of polyamide-based nanocomposites [4,5,40–42], it is well known for PP-based nanocomposites that the layered silicate generally has a mixed morphology consisting of some exfoliated platelets but mostly clay particles consisting of multiple platelets even when PP-*g*-MA is present [4,5,35–37]. Figs. 2 and 3 show TEM micrographs for the current TPO/PP-*g*-MA/MMT nanocomposites as a function of the MMT content and the ratio of PP-*g*-MA to organoclay. All views were taken from the core and viewed parallel to the transverse direction, TD, of injection-molded bars. As the MMT content is increased, the density of MMT particles increases (Fig. 2). The degree of dispersion and exfoliation of the MMT increases as the ratio of PP-*g*-MA/organoclay increases as expected (Fig. 3). A detailed clay particle analysis will be developed in the following section.

Even though there are some reports on the observation of clay particles by AFM [43–45], the usefulness of AFM for investigation of clay particles in nanocomposites is still in question. While TEM micrographs can provide only limited information about the elastomer phase due to the relatively small observable area at the magnifications needed to see the clay particles, identifying elastomer particles using AFM in TPO nanocomposites is relatively easy. Recently, Mirabella et al. [33] and Lee et al. [35,36] reported AFM evidence that addition of organoclay causes a reduction in rubber particle size in PP/elastomer blends.

Fig. 4 shows a series of AFM images for TPO/PP-*g*-MA/MMT nanocomposites as a function of MMT content at a fixed ratio of PP-*g*-MA to organoclay of 1.0. These views are made parallel to the TD of the injection-molded bar. In these AFM images, soft elastomer particles appear dark while the comparatively stiffer PP matrix appears bright. In Fig. 4(a) elastomer particles with dimensions of a few microns are observed for the pure TPO with no clay. A detailed quantitative analysis will be addressed in the next section. The addition of 1 wt% MMT to the TPO leads to a slight reduction in the size of the elastomer particles as shown in Fig. 4(b). Addition of more than 1 wt% MMT leads to dramatic changes in the morphology of these materials, see Fig. 4(c) and (d).

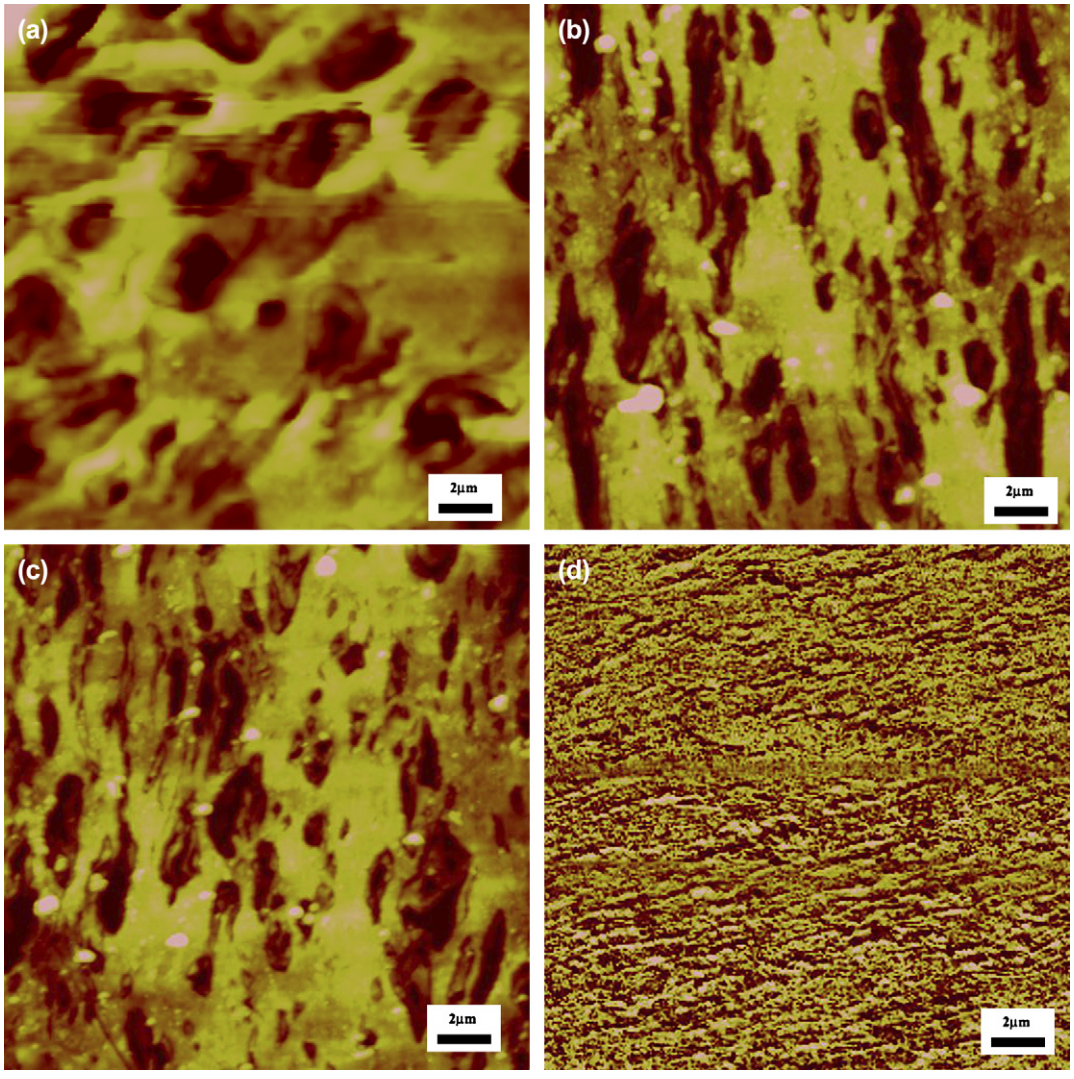

Fig. 4. AFM images of TPO/PP-*g*-MA/MMT nanocomposites revealing rubber morphology as a function of MMT contents of (a) 0, (b) 1, (c) 3, and (d) 7 wt% at a fixed ratio of PP-*g*-MA to organoclay of 1.0. The images are of a microtomed surface in the FD–ND plane taken from the specimen core.

Fig. 5 clearly shows that the elastomer particles are more elongated along the flow direction as the ratio of PP-*g*-MA to organoclay increases at a fixed MMT content of 5 wt%. TPO composites containing 5 wt% MMT without PP-*g*-MA contain elastomer particles with dimensions of a few microns (Fig. 5a), which is not much different than the pure TPO (Fig. 4a). The nanocomposites having a ratio of PP-*g*-MA/organoclay of 0.5 show a mild size reduction and slightly elongated elastomer particles in the flow direction. As the ratio increases, the elastomer particles become more elongated and better dispersed with a more irregular shape in the flow direction as shown in Fig. 5(c) and (d). AFM images of nanocomposites at a ratio of 2.0 reveal even smaller elastomer particles with a more irregular shape (see Fig. 5(d)). These apparent changes in the morphology of the elastomer phase, e.g., decreasing size and increasing irregularity in particle shape as PP-*g*-MA content increases, may stem from two competing effects during melt processing; one is rheological in origin while the other stems from the 'barrier' effect of the clay particles on rubber particle coalescence, which has been discussed in recent publications [35,46].

Fig. 6 illustrates schematically the morphological change in TPO nanocomposites that occurs, based on the TEM and AFM observations shown above, as the PP-*g*-MA/organoclay ratio is increased. As the PP-*g*-MA/organoclay ratio increases, the degree of MMT exfoliation is improved which, in turn, affects the morphology of the rubber particles by interfering with the coalescence process; this reduction in the size of the elastomer particle is believed to be responsible for the enhanced mechanical and thermal expansion properties of these materials. To illustrate more clearly the effect of the clay particles on the size of the elastomer particles, a quantitative analysis of clay and elastomer particle sizes was made from a number of TEM and AFM images.

3.2. Particle analysis for TPO/PP-g-MA/MMT nanocomposites

3.2.1. Clay particles

We recently reported the changes in clay particle morphology for PP-based nanocomposites as the MMT content is

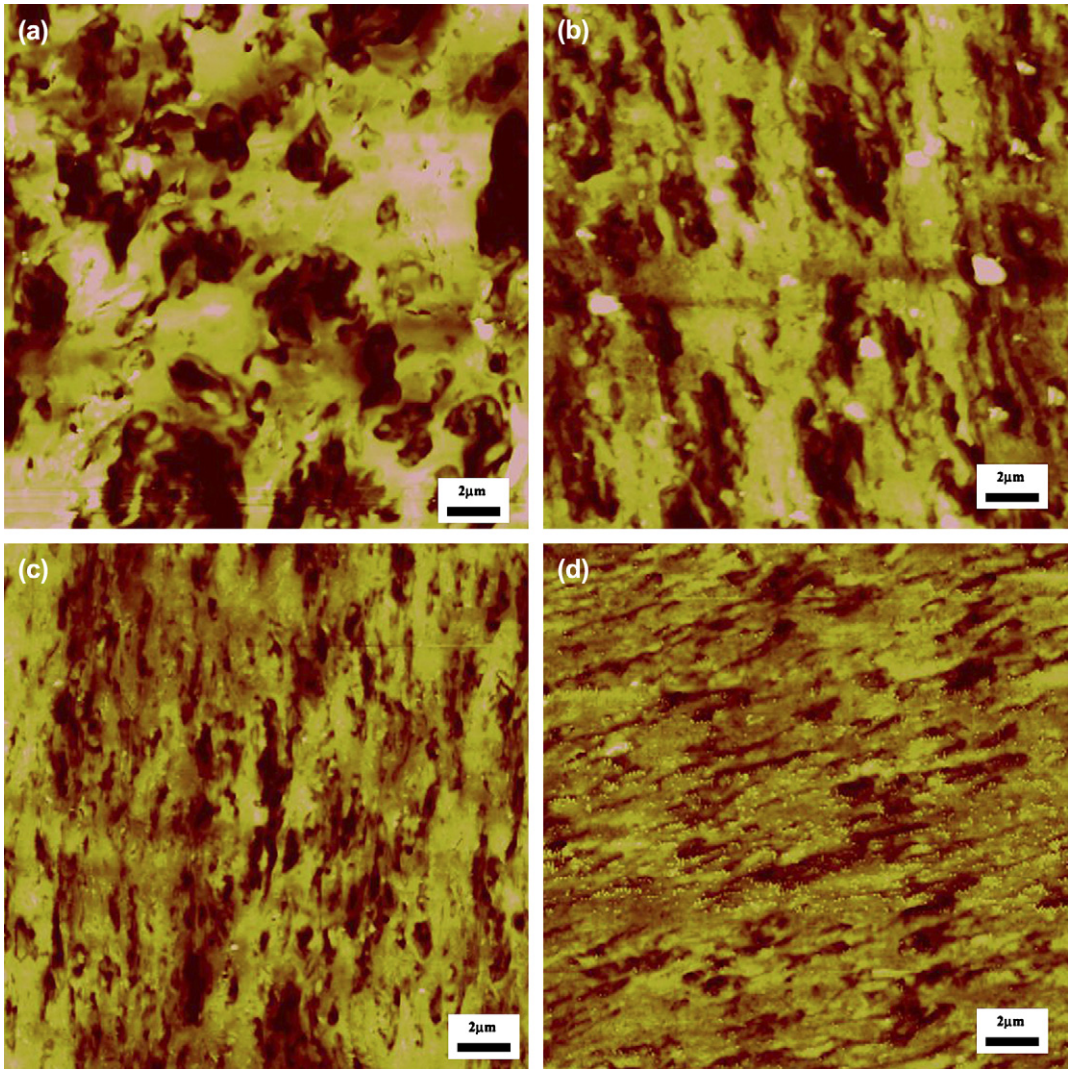

Fig. 5. AFM images of TPO/PP-*g*-MA/MMT nanocomposites showing rubber morphology for PP-*g*-MA to organoclay ratios of (a) 0, (b) 0.5, (c) 1.0, and (d) 2.0 at a fixed MMT of 5 wt%. The images are of a microtomed surface in the FD–ND plane taken from the specimen core.

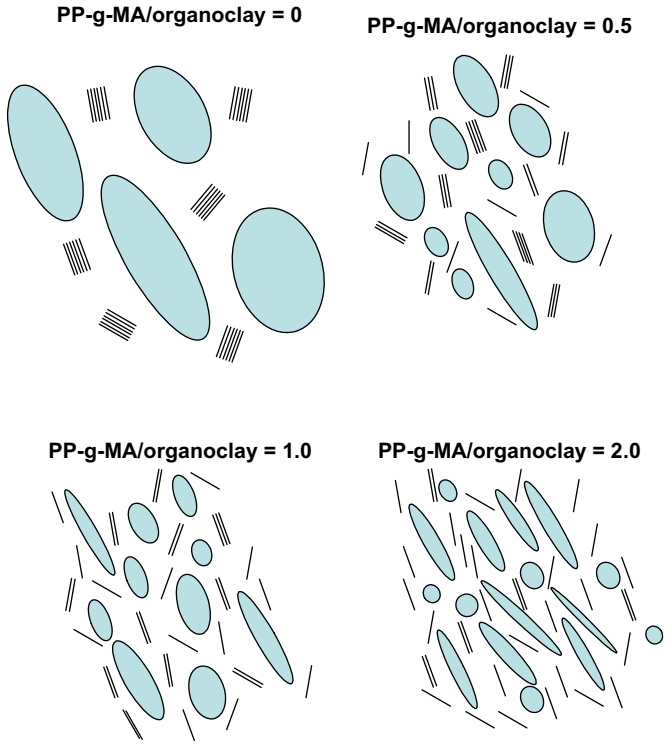

Fig. 6. Schematic illustration of the morphological changes in TPO/PP-*g*-MA/MMT nanocomposites with increasing the ratio of PP-*g*-MA to organoclay at a fixed montmorillonite concentration.

increased at a fixed PP-*g*-MA/organoclay ratio and vice versa [37]. The comparison of length, thickness, and aspect ratio of clay particles for PP nanocomposites and TPO nanocomposites at the same MMT content and PP-*g*-MA/organoclay ratio of 1.0 is summarized in Table 1 and at the same ratio of PP-*g*-MA to organoclay at a fixed MMT content of 5 wt% in Table 2.

Fig. 7 shows histograms that illustrate the distribution of clay particle length, thickness, and aspect ratio obtained from TEM image analysis for TPO nanocomposites containing 5 wt% MMT at a PP-*g*-MA/organoclay ratio of 2.0. In a recent study of PP/masterbatch nanocomposites where the ratio of PP-*g*-MA/organoclay was set at 1.0, Lee et al. [35,36] showed that the particle length decreased with increasing MMT content while the particle thickness increased. Nam et al. reported similar trends in particle length and thickness with varying MMT content for PP-*g*-MA/clay nanocomposites [10]. As a result, the aspect ratio calculated by dividing the average particle length by the average particle thickness decreases as MMT content increases.

We have reported that averaging the aspect ratios of individual particles, $\langle \ell/t \rangle$, leads to values that are generally larger than those calculated from the ratio of average particle length and the average particle thickness, i.e., $\overline{\ell}/\overline{t}$, for PP-based nanocomposites [37]. We have calculated four different aspect ratios represented as $\langle \ell/t \rangle_w$, $\langle \ell/t \rangle_n$, $\overline{\ell}_n/\overline{t}_n$ and $\overline{\ell}_w/\overline{t}_w$, where the subscripts denote number or weight averaging. The current use of the $\langle \ell/t \rangle$ type averaging has been made possible by improved image analysis techniques compared to prior reports from this laboratory [35,36,40–42]. This may be a more appropriate averaging method for modeling properties using theories such as that by Chow as discussed in our previous paper [37]. Results of modeling the properties of these TPO nanocomposites will be reported in a subsequent paper.

Fig. 8 shows the number and weight average clay particle lengths and thicknesses for nanocomposites based on PP and on TPO obtained from TEM views parallel to the TD. The average particle lengths for both PP and TPO nanocomposites decrease while the particle thicknesses increase as MMT content increases. The particle lengths for TPO nanocomposites seem to be lower than that for PP nanocomposites. Furthermore, the particle thickness of the TPO nanocomposites seems to be greater than that measured for PP nanocomposites. Therefore, the aspect ratios, $\langle \ell/t \rangle$, regardless of the averaging method, of TPO nanocomposites are lower than that of PP nanocomposites, as seen in Fig. 9. Interestingly, as clay content is increased, the aspect ratio for PP nanocomposites decreases sharply at low MMT content and does not change further at higher MMT contents; whereas, the aspect ratio of TPO nanocomposites steadily decreases as MMT content increases. This may be due to the presence of the elastomer

Table 1
Image analysis results for clay particles obtained from TEM micrographs of injection-molded PP/PP-*g*-MA/MMT nanocomposites and TPO/PP-*g*-MA/MMT nanocomposites at a fixed PP-*g*-MA/organoclay ratio of 1.0 (viewed parallel to the TD)

	PP/PP-*g*-MA/MMT				TPO/PP-*g*-MA/MMT			
MMT concentration (wt%)	0.97	3.0	5.4	7.4	0.84	2.6	4.7	6.8
Number average particle length (nm), $\overline{\ell}_n$	238	217	173	175	178	165	152	134
Weight average particle length (nm), $\overline{\ell}_w$	268	304	206	215	222	225	185	178
Number average particle thickness (nm), $\overline{t}_n$	4.8	5.7	4.9	5	5.1	5.6	5.8	5.7
Weight average particle thickness (nm), $\overline{t}_w$	6.1	9.5	7.8	10.3	8.2	10.4	10.9	10.8
Number average aspect ratio $\langle \ell/t \rangle_n$	56	45	44	43	46	40	38	32
Weight average aspect ratio $\langle \ell/t \rangle_w$	67	54	56	53	63	59	51	43
Aspect ratio, $\overline{\ell}_n/\overline{t}_n$	49	38	35	35	35	29	26	24
Aspect ratio, $\overline{\ell}_w/\overline{t}_w$	44	32	26	21	27	22	17	17

Table 2
Image analysis results for clay particles obtained from TEM micrographs of injection-molded PP/PP-*g*-MA/MMT nanocomposites and TPO/PP-*g*-MA/MMT nanocomposites at a fixed MMT content of 5 wt% (viewed parallel to the TD)

	PP/PP-*g*-MA/MMT				TPO/PP-*g*-MA/MMT			
PP-*g*-MA/organoclay	0	0.5	1.0	2.0	0	0.5	1.0	2.0
Number average particle length (nm), $\bar{\ell}_n$	634	233	173	181	623	161	151	143
Weight average particle length (nm), $\bar{\ell}_w$	860	317	206	224	1553	214	185	187
Number average particle thickness (nm), $\bar{t}_n$	101	11.3	4.9	3.8	84.0	13.9	5.8	4.1
Weight average particle thickness (nm), $\bar{t}_w$	143	16.1	7.8	4.4	134.6	21.3	10.9	7.5
Number average aspect ratio $\langle \ell/t \rangle_n$	7	25	44	51	9	16	38	43
Weight average aspect ratio $\langle \ell/t \rangle_w$	10	38	56	63	10	34	51	52
Aspect ratio, $\bar{\ell}_n/\bar{t}_n$	6	21	35	48	12	12	26	35
Aspect ratio, $\bar{\ell}_w/\bar{t}_w$	6	20	26	51	7	10	17	25

phase in the TPO nanocomposites. The increase in melt viscosity by the dispersion of clay particles affects the dispersion of the elastomer phase. More importantly, the clay particles retard the coalescence of elastomer phase as discussed recently [35,36,46]. On the other hand, the presence of the elastomer phase seems to suppress the dispersion of clay platelets.

Recently, several groups have shown that organoclays can effectively reduce the domain size of polymer blends in several systems. The literature proposes several reasons for this effect. It has been suggested that the organoclay locates in the interface and/or encapsulates the dispersed phase and acts like a compatibilizer for blends of PMMA/PS [47,48], PP/PS [49,50], PC/ABS or ABS/PA6 [51] and PET/PE [52]. Others attribute this effect to the clay acting as a physical barrier that retards the coalescence of the dispersed phases for Nylon 6/EPR [46], PA6/PP [53,54], and Nylon 6/LLDPE [55] blend systems. In the latter, the organoclay does not seem to be located at the interface. We believe that the role of organoclay depends on the blend system and is affected by the blend composition, the relative affinity between the polymers and the organoclay, processing conditions, etc. However, elucidating these details is beyond the scope of this study. For the current nanocomposites, the organoclay seems to act as a physical barrier that slows down the rate of coalescence of elastomer particles. While the well-dispersed organoclay retards the coalescence of the elastomer particles, the presence of elastomer seems to suppress the dispersion of clay platelets. This may cause the reduction of particle aspect ratio in TPO nanocomposites compared to that in PP matrix as shown in Fig. 9.

3.2.2. Elastomer particles

Particle analysis for the elastomer phase in TPO/PP-*g*-MA/MMT nanocomposites is quite complex due to the nonspherical nature of the particles as shown in the AFM images. To determine the size of the elastomer particles, the image analysis software used identifies each individual elastomer particle and evaluates its area, A, plus its dimensions along the major and minor axes [35,36]. For simple comparison among nanocomposites, an apparent elastomer particle size, d, was calculated using the following relation.

$$d = \left(\frac{4A}{\pi}\right)^{1/2} \tag{1}$$

A series of histograms of apparent elastomer particle sizes defined by Eq. (1), see Fig. 10, were built for the TPO nanocomposites at a fixed MMT content of 5 wt% and various ratios of PP-*g*-MA to organoclay. From the distribution of elastomer particle sizes shown in the histograms, the number and weight averages of the apparent particle size, d, and dimensions along the major, l, and minor, $\boldsymbol{t}$, axes are calculated as follows:

$$\bar{d}_n = \frac{\sum n_i d_i}{\sum n_i}, \quad \bar{l}_n = \frac{\sum n_i l_i}{\sum n_i} \tag{2}$$

$$\bar{d}_w = \frac{\sum n_i d_i^2}{\sum n_i d_i}, \quad \bar{l}_w = \frac{\sum n_i l_i^2}{\sum n_i l_i} \tag{3}$$

where n_i is the number of elastomer particles within fixed increments of d_i and l_i. Similar averages were computed for $\boldsymbol{t}$. No attempt was made to convert apparent particle sizes into true particle sizes due to the complex nature of the particle shape, especially for nanocomposites containing high MMT loadings. The interparticle distance, ID, sometimes referred to as the matrix ligament thickness, can be calculated from the following equation [35,56]:

$$\mathrm{ID} = d\left[\left(\frac{\pi}{6\phi_r}\right)^{1/3} - 1\right] \tag{4}$$

where ϕ_r is the dispersed particle volume fraction and d is the average particle diameter. The apparent particle size, $\bar{\boldsymbol{d}}_w$, was used to calculate the ID values shown in Tables 3 and 4.

Tables 3 and 4 summarize the elastomer particle size analyses for a series of TPO nanocomposites as a function of

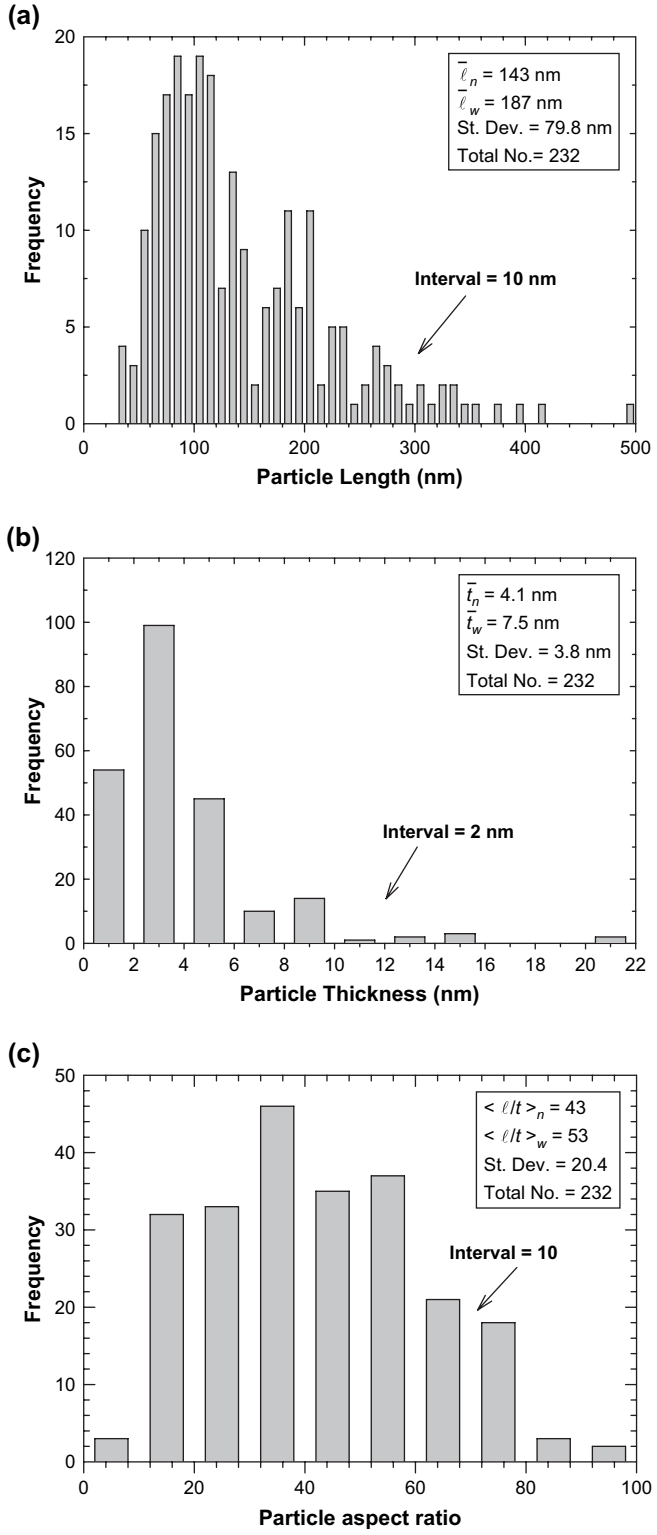

Fig. 7. Histogram of MMT particle lengths, thicknesses and aspect ratios for TPO/PP-*g*-MA/MMT nanocomposites at a PP-*g*-MA/organoclay ratio of 2.0, viewed parallel to TD (MMT content = 5 wt%).

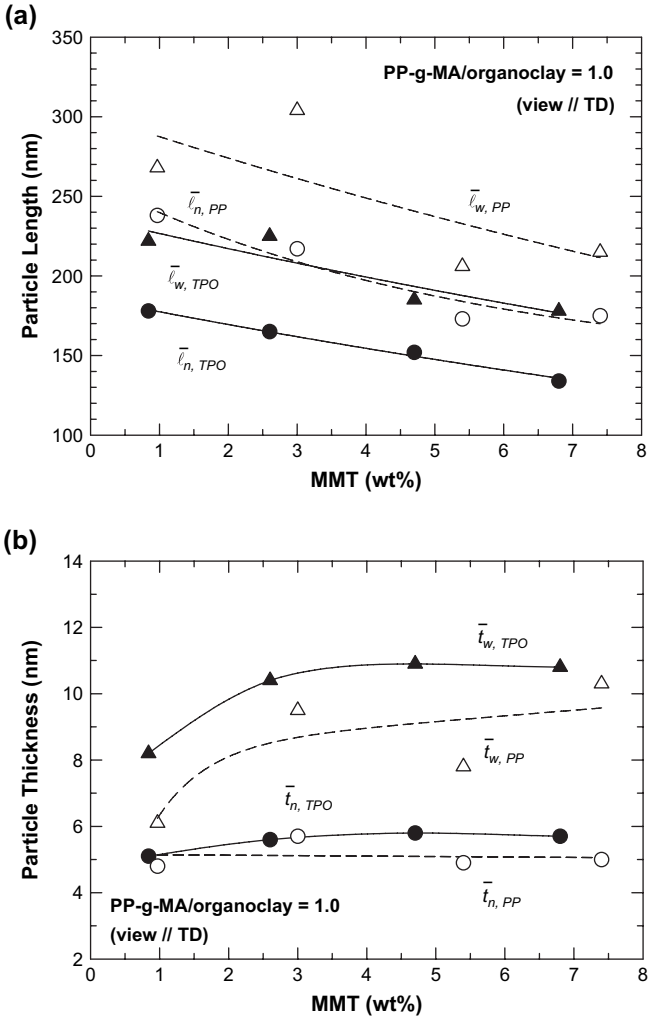

Fig. 8. Effect of MMT content on (a) clay particle length and (b) clay thickness of PP nanocomposites and TPO nanocomposites for a PP-*g*-MA/organoclay ratio of 1.0.

MMT content and various ratios of PP-*g*-MA to organoclay. Fig. 11(a) shows the weight average apparent particle sizes as a function of MMT content measured from AFM images viewed parallel to the TD. The average elastomer particle length measured along the FD decreases with the addition of MMT. The weight average elastomer particle size in the TPO without clay is 1.16 μm; this is somewhat smaller than that in the PP/elastomer blend containing 30% elastomer (2.83 μm) reported by Lee et al. [35,36]. It is noted that this reactor-made TPO seems to have smaller elastomer particles than that obtained by blending PP and elastomer in a twin screw extruder. This issue will be addressed more fully elsewhere. Without PP-*g*-MA, the weight average apparent elastomer particle size is 1.01 μm at a fixed MMT content of 5 wt%, see Fig. 11(b). In the nanocomposites where the ratio of PP-*g*-MA to organoclay is 0.5, the elastomer particle size is similar to that of TPO/MMT composites (1.01 μm). As the PP-*g*-MA/organoclay ratio increases from 0.5 to 1.0, the elastomer particle size is significantly reduced (0.63 μm) but it does not change much as this ratio is further increased.

AFM views in the TD direction give similar trends for the average lengths along the major and minor axes, $\bar{l}$ and $\bar{t}$, of the elastomer particles, i.e., $\bar{l}$ decrease slightly but $\bar{t}$ decrease more significantly with the addition of clay, see Fig. 12(a). However,

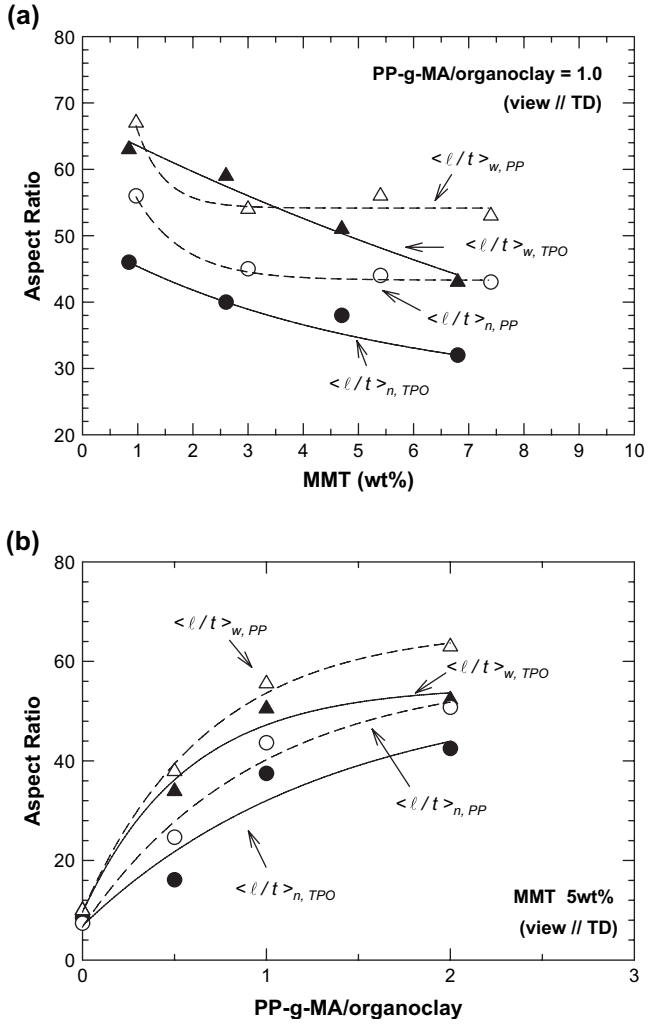

Fig. 9. Effect of MMT content on clay particle aspect ratio for PP nanocomposites and TPO nanocomposites at various (a) MMT contents and (b) PP-*g*-MA/organoclay ratios.

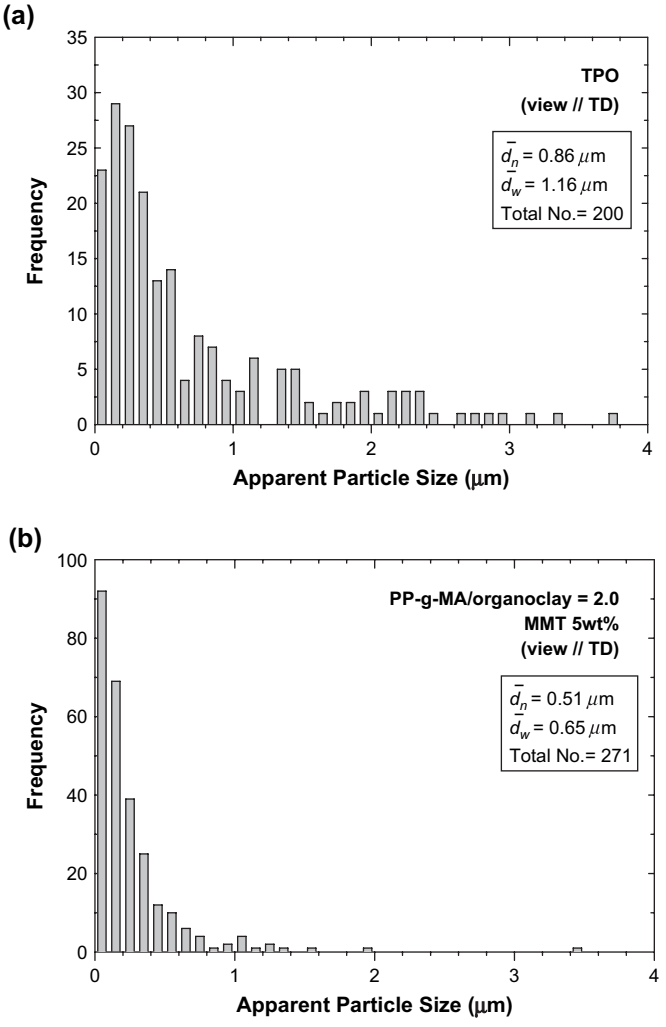

Fig. 10. Histograms of apparent elastomer particle size data obtained by analyzing AFM images of (a) TPO and (b) TPO/PP-*g*-MA/MMT nanocomposites with PP-*g*-MA to organoclay ratios of 2.0 at a fixed MMT content of 5 wt%.

the weight average elastomer particle aspect ratio, i.e., major length/minor length of a particle, $\langle l/t \rangle$, or $\bar{l}/\bar{t}$ within a given viewing plane increases dramatically, see Fig. 13(a), as the apparent particle size decreases for the current nanocomposites, as shown in Table 3. This may stem from the nature of the ''barrier'' effect caused by the presence of the clay particles and their influence on elastomer particle orientation (or stretching) during the injection molding process. It should be noted that the aspect ratios calculated by averaging the values for individual particles, $\langle l/t \rangle$, are generally larger than those calculated from the ratio of the average particle length and the average particle thickness, $\bar{l}/\bar{t}$, similar to the case for clay particles.

The elastomer particle dimensions along the major or minor axes show fairly similar trends as the ratio of PP-*g*-MA to organoclay increases at a fixed MMT content, as shown in

Table 3
Elastomer particle size comparison for TPO/PP-*g*-MA/MMT nanocomposites for different MMT contents at a fixed ratio of PP-*g*-MA/organoclay of 1.0

MMT (wt%)	Total Number of particles	Particle size (μm)		Major length (μm)		Minor length (μm)		ID (μm)	Elastomer aspect ratio			
		$\bar{d}_n$	$\bar{d}_w$	$\bar{l}_n$	$\bar{l}_w$	$\bar{t}_n$	$\bar{t}_w$		$\langle l/t \rangle_n$	$\langle l/t \rangle_w$	$\bar{l}_n/\bar{t}_n$ [a]	$\bar{l}_w/\bar{t}_w$ [b]
TPO	200	0.86	1.16	1.26	1.82	0.62	0.88	0.42	2.12	2.41	2.03	2.07
1	211	0.60	0.86	0.87	1.55	0.44	0.69	0.31	2.07	2.60	1.98	2.24
3	179	0.58	0.84	0.99	1.68	0.35	0.52	0.31	2.94	3.92	2.81	3.25
5	255	0.53	0.77	0.99	1.46	0.28	0.33	0.28	3.98	5.24	3.48	4.45
7	298	0.55	0.64	1.14	1.50	0.26	0.31	0.23	4.75	6.28	4.40	4.85

[a] The values of the aspect ratio were computed from the number average particle length and thickness.
[b] The values of the aspect ratio were computed from the weight average particle length and thickness.

Table 4
Elastomer particle size comparison for TPO/PP-*g*-MA/MMT nanocomposites for different ratio of PP-*g*-MA/organoclay at a fixed MMT content of 5 wt%

(PP-*g*-MA/organoclay)	Total Number of particles	Particle size (μm)		Major length (μm)		Minor length (μm)		ID (μm)	Elastomer aspect ratio			
		$\bar{d}_n$	$\bar{d}_w$	$\bar{l}_n$	$\bar{l}_w$	$\bar{t}_n$	$\bar{t}_w$		$\langle l/t\rangle_n$	$\langle l/t\rangle_w$	$\bar{l}_n/\bar{t}_n$ [a]	$\bar{l}_w/\bar{t}_w$ [b]
0	150	0.78	1.01	1.33	1.95	0.56	0.76	0.37	2.4	2.9	2.17	2.22
0.5	163	0.76	1.01	1.2	1.69	0.47	0.65	0.37	3.02	3.74	2.81	3.03
1.0	255	0.53	0.77	0.99	1.46	0.28	0.33	0.28	3.98	5.24	3.48	4.45
2.0	271	0.51	0.65	1.04	1.7	0.26	0.35	0.24	4.42	6.53	3.93	4.82

[a] The values of the aspect ratio were computed from the number average particle length and thickness.
[b] The values of the aspect ratio were computed from the weight average particle length and thickness.

Fig. 12(b). The average elastomer particle aspect ratios within a given viewing plane increase as the PP-*g*-MA contents increases, see Fig. 13(b). At a low ratio of PP-*g*-MA to organoclay, e.g., 0.5, the dispersion state of the clay is poor and clay particles do little to prevent coalescence of elastomer particles, see Figs. 3(b) and 5(b). However, the well-dispersed and oriented clay particles along the FD promoted by a higher PP-*g*-MA/organoclay ratio are much more effective in preventing the coalescence of the elastomer particles and in distorting the shape of the elastomer domains, see Figs. 3(d) and 5(d). The deformed elastomer particles in molded specimens may play an important role in the thermal expansion behavior and to some extent mechanical properties for nanocomposites where the directional dependence of properties is already great.

For rubber-toughened polymers, a brittle–ductile transition generally can be induced either by increasing elastomer content or by decreasing elastomer particle size [56–58]. Jiang

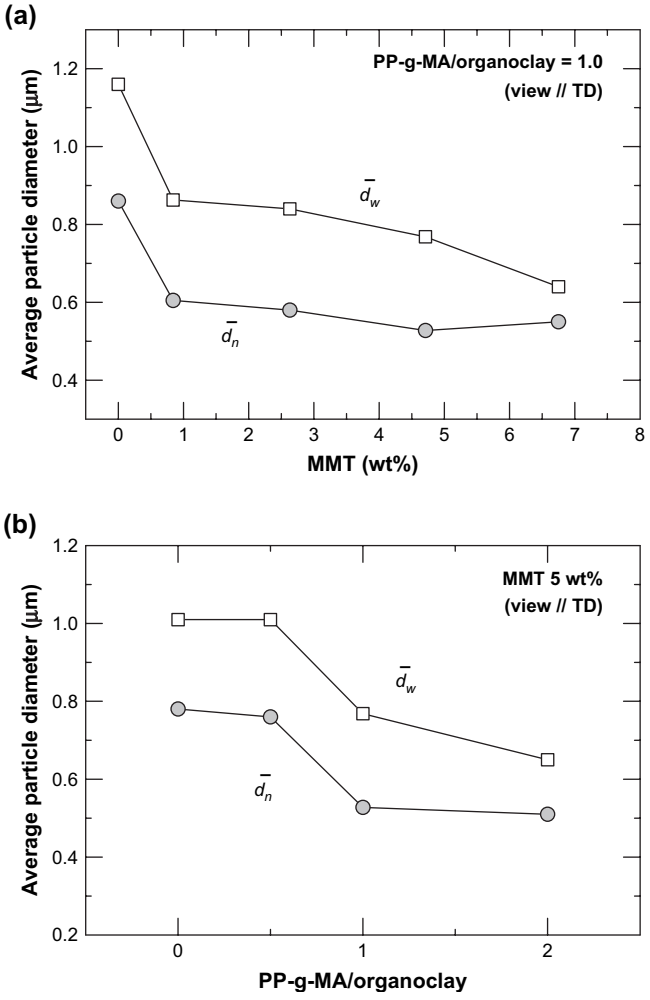

Fig. 11. Elastomer particle size as seen in views parallel to TD for TPO/PP-*g*-MA/MMT nanocomposites: (a) at a PP-*g*-MA/organoclay ratio of 1.0 and (b) at a fixed MMT contents of 5 wt%.

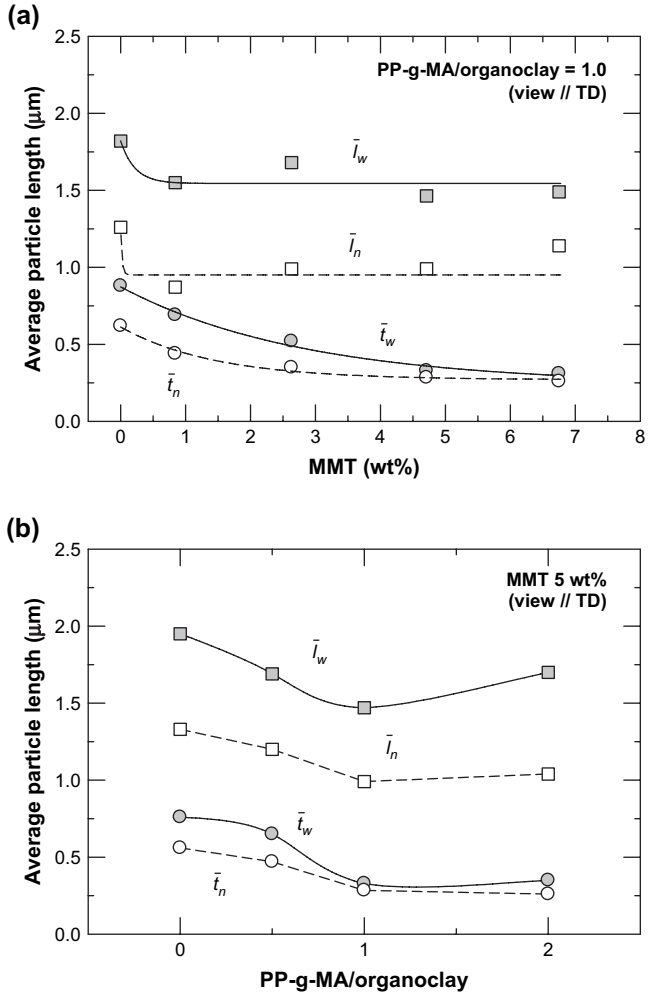

Fig. 12. Elastomer particle length and thickness as seen in views parallel to TD for TPO/PP-*g*-MA/MMT nanocomposites: (a) at a PP-*g*-MA/organoclay ratio of 1.0 and (b) at a fixed MMT content of 5 wt%.

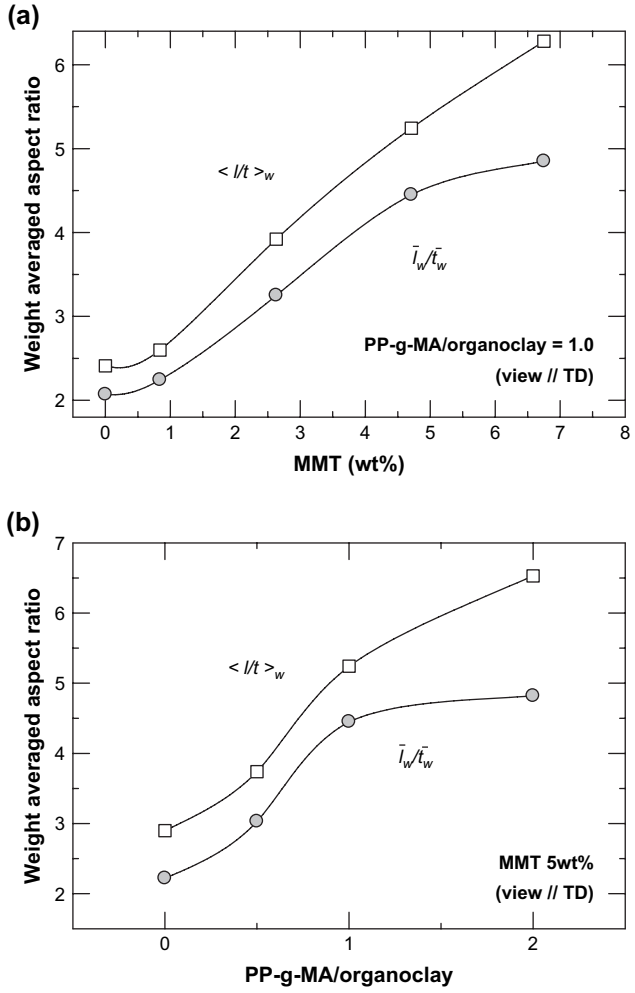

Fig. 13. Aspect ratio of elastomer particles as seen in views parallel to TD for TPO/PP-*g*-MA/MMT nanocomposites: (a) at a PP-*g*-MA/organoclay ratio of 1.0 and (b) at a fixed MMT content of 5 wt%.

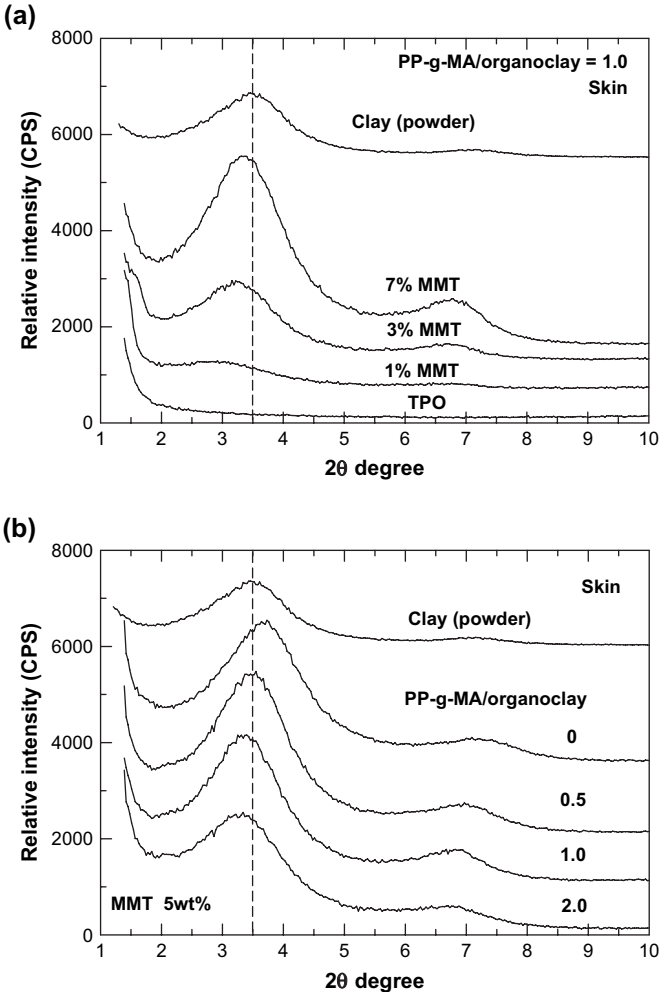

Fig. 14. WAXS scans for TPO/PP-*g*-MA/MMT nanocomposites.

et al. [58,59] interpreted the transition seen in PP/rubber blends caused by increasing rubber content at essentially fixed particle size (0.5–0.8 μm) in terms of the decrease in the interparticle distance. They reported a critical interparticle distance of 0.15 μm at 25 °C for PP/EPDM blends. Lee et al. [35] showed that the fracture behavior of PP nanocomposites containing 30 wt% elastomer undergoes a brittle–ductile transition as the amount of MMT changes from 1 to 2.8 wt%. The nanocomposite containing 2.8 wt% of MMT is super-tough (>600 J/m) while the one containing 1 wt% of MMT is relatively brittle (~100 J/m). This apparent toughening may be attributed to the decrease in the elastomer particle size and/or interparticle distance to below a critical value that induces the brittle–ductile transition [57,58]. In this case, the critical value of apparent particle size for toughening lies between 1.0 and 1.5 μm and the critical interparticle distance is of the order of 0.2–0.3 μm; however, these values should be considered as relative ones since the toughening mechanism for PP/rubber blends is known to be dependent on the rubber characteristics [26] and, no doubt, are affected also by the reinforcement due to clay particles. For the current nanocomposites, the elastomer size for the reactor-made TPO is 1.16 μm and its interparticle distance is 0.42 μm as shown in Table 3. This particle size lies in a range where toughness might be expected; however, the interparticle distance is larger than that might be expected for good toughness [35]. We believe that the reactor-made TPO containing about 25 wt% of elastomer has been well-optimized for toughness; it shows super-tough behavior (>600 J/m) while the extruder-made PP/elastomer blend containing 30 wt% of elastomer has a much lower fracture energy (~100 J/m). By adding the filler and/or PP-*g*-MA, the elastomer particle size and interparticle distance decrease to 0.64 and 0.23 μm, respectively, for the current TPO nanocomposite with 7 wt% MMT at a fixed PP-*g*-MA/organoclay ratio of 1.0 (see Table 3). The relationship between morphology and toughness will be discussed more fully in Section 3.4.

3.3. WAXS scan for nanocomposites

Fig. 14 compares WAXS scans for the organoclay and for the TPO nanocomposites with different clay concentrations and PP-*g*-MA/organoclay ratios. The neat organoclay shows

an intense peak at around $2\theta = 3.6°$, corresponding to a basal spacing of 24.2 Å. The scans taken from the skin portion of the injection-molded specimens, Fig. 14(a), reveal that a strong peak from the organoclay persists in these nanocomposites without any significant shift in location; however, the intensity of this peak increases with increasing MMT content, indicating that large stacks of platelets exist in the skin portion of injection-molded specimens. As pointed out by Lee et al., the situation may be rather different in the core of the specimen owing to differences in the dispersion and orientation states of clay particles between the skin and the core [35]. Interestingly, the peak for TPO/organoclay composites without PP-*g*-MA appears to be shifted to a slightly higher angle. This could mean a collapse of the interlayer (see Fig. 14(b)). The X-ray peak characteristic of the organoclay seems to be shifted very slightly to higher angles in some cases and to lower angles in others. As discussed in a previous paper [37], these differences are so small that it is risky to attach much physical meaning to them. The WAXS results say very little about morphology except that exfoliation is not complete, even then this technique can lead to false and incomplete interpretations for nanocomposites. Direct observation by TEM is needed for a better understanding of the state of dispersion [19,60,61]. However, the main problem with TEM is that the volume probed is very small and may not be representative of the nanocomposite as a whole. Therefore, bulk properties such as rheological/mechanical properties should be analyzed in conjunction with TEM and WAXS observations.

3.4. Mechanical properties

Fig. 15(a) shows the effect of the MMT content on the tensile modulus of TPO nanocomposites, E, for various PP-*g*-MA/organoclay ratios. The addition of MMT to TPO with PP-*g*-MA results in a substantial increase in stiffness, especially at low MMT concentrations, i.e., <2–3%. Interestingly, the rate of tensile modulus increase is quite strong up to a PP-*g*-MA/organoclay ratio of one, but beyond this the benefit is much less as shown in Fig. 15(b). As reported in most of the literature, PP-*g*-MA is needed to achieve better dispersion of the silicate platelets in a PP or TPO matrix, and as a consequence, improved stiffness of the nanocomposites. The effect of the PP-*g*-MA content on the tensile modulus of TPO nanocomposites is much more significant than for PP-based nanocomposites (see the previous paper [37]). The presence of the elastomer phase in the TPO lowers the modulus of the "matrix" phase, E_m, which increases the propensity for reinforcement by the filler, i.e., an increase in E/E_m, as predicted by composite theory. It is important to note that PP-*g*-MA has a considerably lower modulus than pure PP; thus, even though better exfoliation and orientation of the clay are achieved by adding PP-*g*-MA, the absolute modulus of PP nanocomposites is not improved as much as expected because of the reduction of E_m. In the case of TPO, where the modulus is lowered by the elastomer, addition of PP-*g*-MA does not reduce the matrix properties as much as it does in PP.

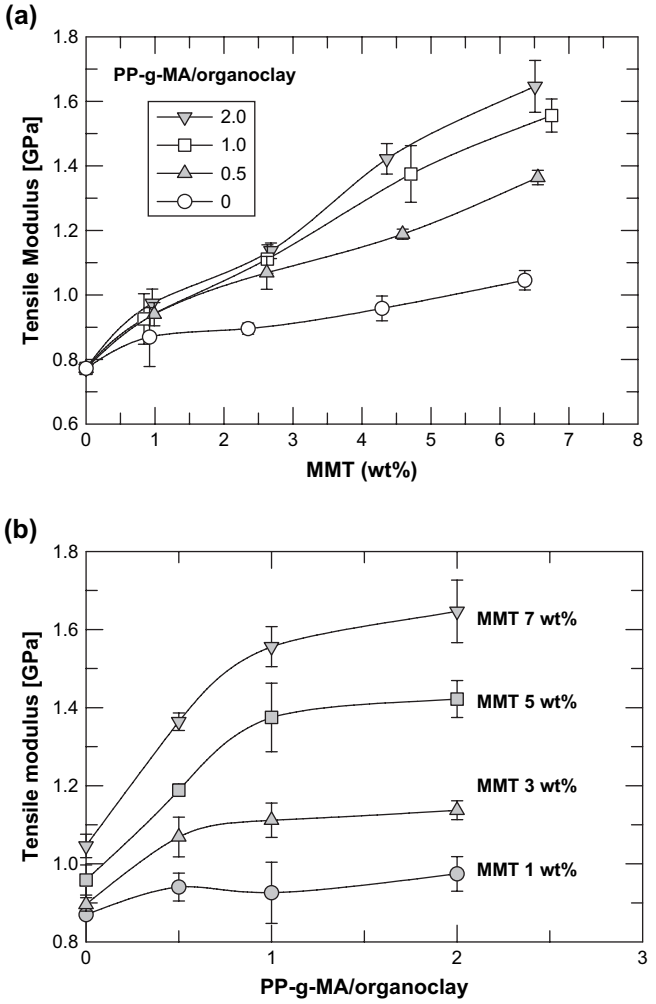

Fig. 15. Effect of PP-*g*-MA content on the tensile modulus of TPO nanocomposites as (a) a function of the montmorillonite content and (b) the ratio of PP-*g*-MA to organoclay at a test speed of 0.51 cm/min.

Fig. 16 shows the effect of the amount of PP-*g*-MA on the tensile modulus and the impact strength of TPO/PP-*g*-MA blends without any clay. While the tensile modulus of PP/PP-*g*-MA blends can be reduced by ~15% with 24 wt% of PP-*g*-MA, significantly less reduction is observed when a TPO matrix is used. The modulus reduction does not exceed ~5% at the highest PP-*g*-MA level used. Additionally, the presence of PP-*g*-MA itself does not seem to have a significant effect on the toughness of the TPO. As seen in Fig. 16(b), TPO/PP-*g*-MA blends without MMT show the super-tough behavior (>600 J/m) in the range of compositions used in this study.

Fig. 17 shows the effect of MMT content on the yield strength of TPO nanocomposites for various PP-*g*-MA/organoclay ratios. In the case of TPO/MMT composites without any compatibilizer (ratio = 0), the yield strength shows an initial increase and then decreases as the MMT content increases further. However, the yield strength, in general, increases with MMT content for TPO/PP-*g*-MA/MMT nanocomposites. The effect of PP-*g*-MA content on yield strength is much more

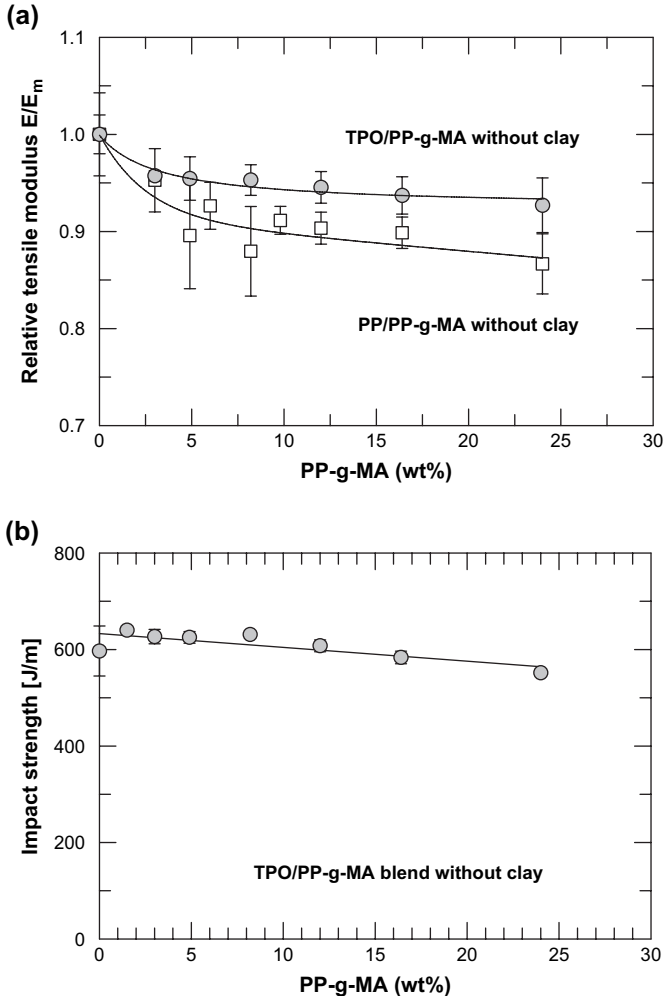

Fig. 16. (a) Tensile modulus and (b) impact strength of TPO/PP-*g*-MA blends without clay.

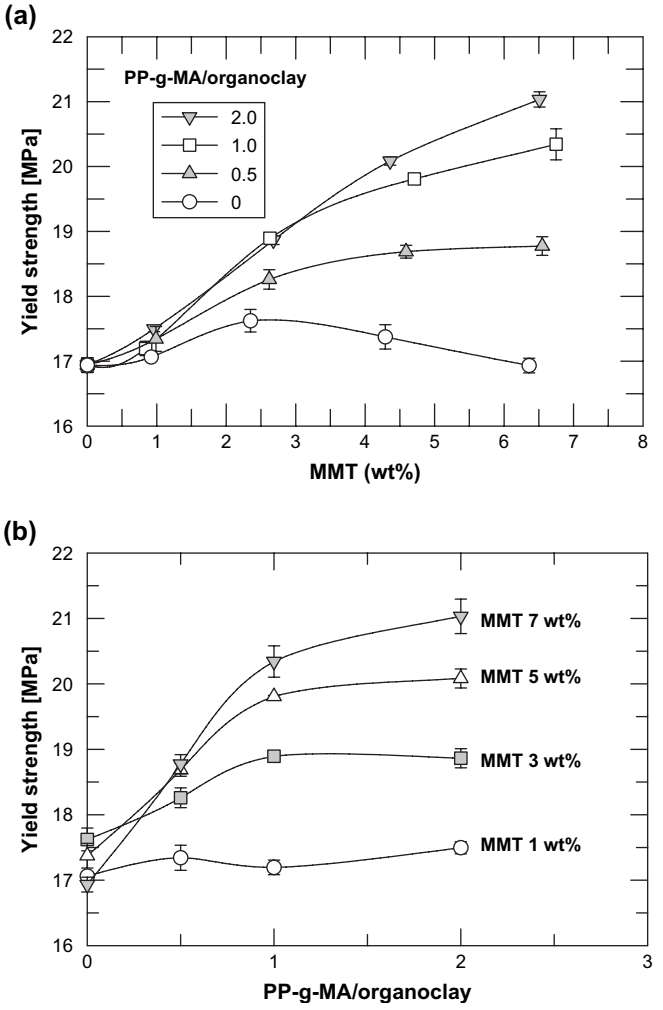

Fig. 17. Yield strength of TPO nanocomposites as a function of (a) the montmorillonite content and (b) the ratio of PP-*g*-MA to organoclay at a test speed of 5.1 cm/min.

clearly shown in Fig. 17(b). Interestingly, the rate of increase of the yield strength with clay concentration is much more pronounced at higher PP-*g*-MA contents particularly at higher clay contents. This may be related to better interfacial adhesion between the clay particles and the TPO matrix in addition to the increased dispersion and exfoliation of the clay platelets as the PP-*g*-MA content increases.

The values of elongation at yield and break for TPO nanocomposites are shown in Fig. 18. The elongation at yield decreases slightly at low MMT concentrations, i.e., 1 wt% (Fig. 18a), and then increases as MMT loading increases. The elongation at break exhibits a minimum at low MMT content and then a maximum at higher MMT loadings (Fig. 18c). The elongations at yield and break show a maximum at low PP-*g*-MA contents and then decrease as the PP-*g*-MA content increases further (Fig. 18b and d). This may reflect changes in both clay and elastomer particle morphology.

Fig. 19 shows the influence of the MMT and the PP-*g*-MA content on the notched Izod impact strength. Values from the far and gate ends of injection-molded samples were averaged since the difference between the two is relatively small. Lee et al. [35] reported that the fracture goes from brittle to ductile as the amount of MMT exceeds a certain value for PP/elastomer/masterbatch nanocomposites at high contents of elastomer, e.g., 30 and 40%, at a PP-*g*-MA/organoclay ratio of 1.0. This is opposite to the trend for the current nanocomposites where there is a decrease in impact strength as the amount of filler increases. In the prior case, the rubber particles in the PP/elastomer blend were too large to give good toughening when no nanomaterial was present; thus, the addition of organoclay led to increased toughness because it brought the rubber particle size into a better range. This increase in toughening occurred in spite of the reinforcement effect that generally decreases ductility and toughness. For the current nanocomposites, the reactor-made TPO has a more optimum rubber particle size as was previously mentioned. By adding organoclay and PP-*g*-MA, the rubber particles may be reduced below the optimum size. This may lead to some loss in toughness as shown in Fig. 19, but we believe that the reduction in Izod impact strength is mainly related to the reinforcement effect.

Without any PP-*g*-MA (ratio = 0), the value of the Izod impact strength decreases slightly as MMT content increases. Apparently, the presence of PP-*g*-MA without clay or clay

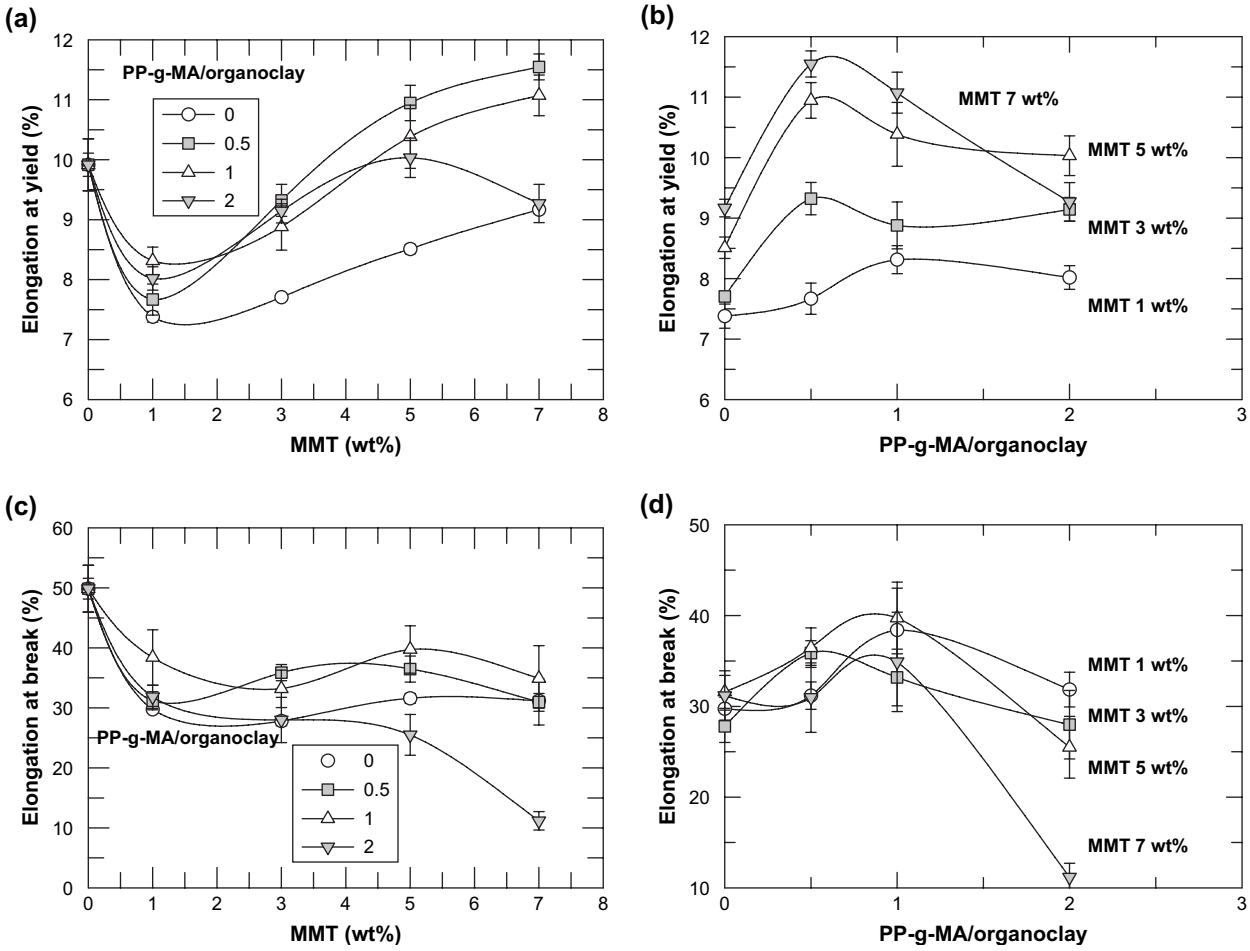

Fig. 18. Effect of montmorillonite content and PP-*g*-MA to organoclay ratio on (a and b) elongation at yield and (c and d) elongation at break for TPO/PP-*g*-MA/MMT nanocomposites at a test speed of 5.1 cm/min.

without PP-*g*-MA, does not significantly affect the toughness of TPO. It is important to note that PP-*g*-MA does not seem to act like a compatibilizer between the elastomer and the PP matrix as it does for polyamide blends with polypropylene [53] or ethylene–propylene elastomer [62]. While the stiffness of TPO decreases slightly as PP-*g*-MA is added due to its lower crystallinity, the super-tough behavior of the TPO is maintained (see Fig. 16). This reflects the fact that PP-*g*-MA does not significantly affect the morphology of the dispersed elastomer phase in the TPO or its intrinsic ability to toughen the PP matrix. In addition, organoclay used without PP-*g*-MA does not seem to affect the stiffness or toughness of the TPO. It appears that the organoclay does not reside at the elastomer–PP matrix interface in this system. Even though the stiffness of the TPO increases marginally at the expense of the toughness (which is still over 500 J/m with 7 wt% of MMT (see Fig. 16b)), as clay is added, the effect of the clay without PP-*g*-MA appears negligible.

Returning to Fig. 19, the Izod values in general decrease more as the MMT content increases for higher contents of PP-*g*-MA. This apparently stems from the better exfoliation or improved dispersion of the clay particles throughout the matrix as the amount of PP-*g*-MA increases. Interestingly, the fracture energy of TPO improves with the addition of 1 wt% of MMT for all of the nanocomposites that were evaluated (see Fig. 19(a)). This improvement in the Izod value may reflect the increased stiffness and yield strength of the materials, which offset the negative effects of decreased ductility, i.e., reduced extent of plastic deformation, as discussed by Shah et al. [63]. However, at high clay concentrations with PP-*g*-MA, the decreased ductility seems to dominate and the toughness decreases. The Izod impact strength clearly decreases as the amount of PP-*g*-MA increases, see Fig. 19(b), at higher MMT contents like 5 and 7 wt%. At a PP-*g*-MA/organoclay ratio of 2.0, fracture goes from ductile to brittle with complete breakage of the specimen during the impact test as shown in Fig. 20. However, it is significant to note that these materials exhibit ductile failure except at the highest levels of PP-*g*-MA and MMT. The samples that fail in a ductile manner exhibit hinged breaks and high Izod values; whereas, samples that fail in a brittle manner exhibit complete breaks and low Izod values.

3.5. Rheological properties

The melt rheological properties of nanocomposites can provide fundamental insights about the processability and

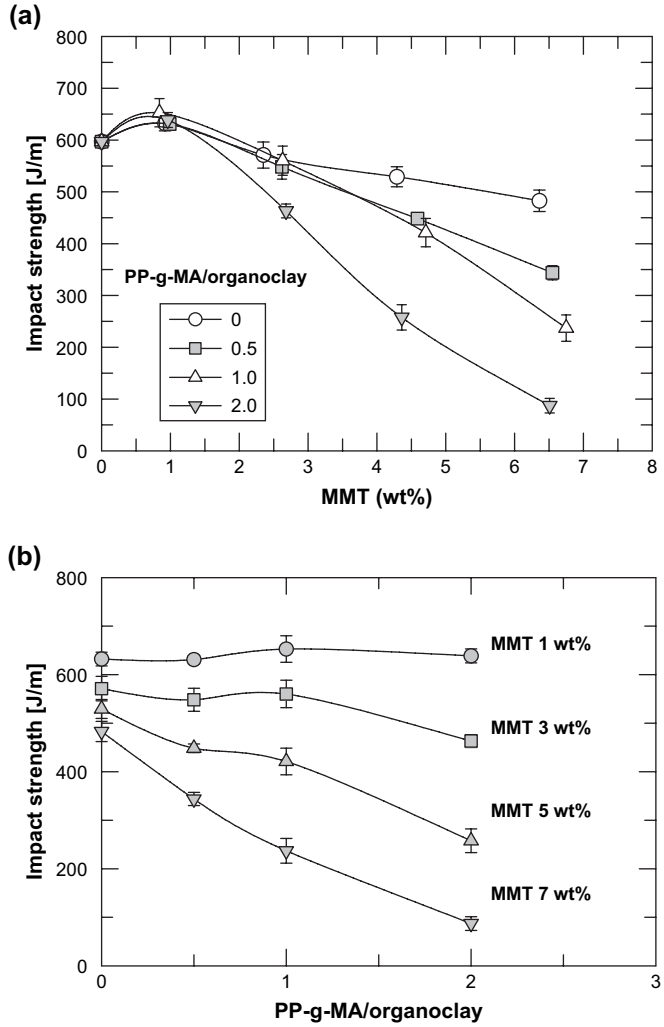

Fig. 19. Notched Izod impact strength as a function of (a) the montmorillonite content and (b) PP-*g*-MA to organoclay ratio.

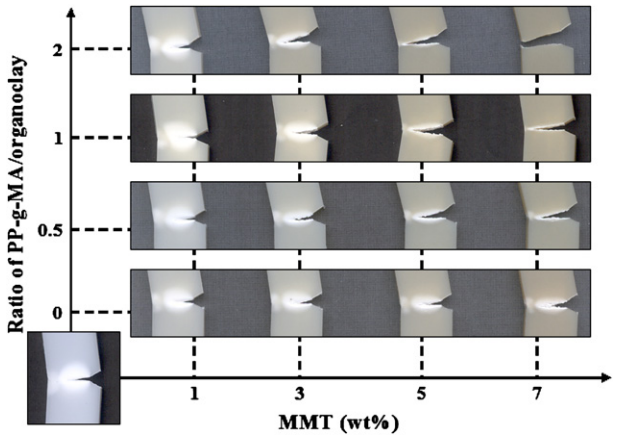

Fig. 20. Photographs of Izod specimens taken after the notched impact test for the TPO/PP-*g*-MA/MMT nanocomposites at different ratios of PP-*g*-MA to organoclay (far end samples only).

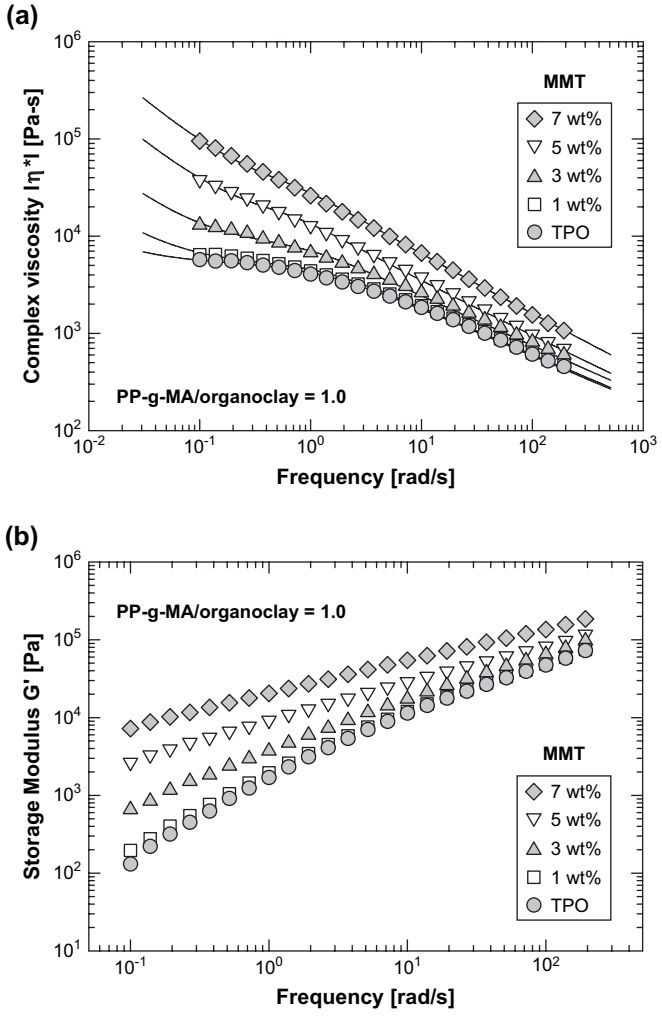

Fig. 21. Frequency sweep results for TPO nanocomposites at 180 °C. (a) Complex viscosity and (b) storage modulus at different MMT contents at a fixed PP-*g*-MA/organoclay ratio of 1.0. Solid line indicates the empirical fitting of complex viscosity with Eq. (5).

morphology of these materials. Viscoelastic measurements are highly sensitive to the nanoscale and mesoscale structures of the nanocomposites and appear to be a powerful method to probe the state of dispersion in such materials [15,64–66]. The enhancement of the rheological properties is generally attributed to percolated networks caused by the physical interaction of the clay platelets. There is a significant lowering of the percolation threshold, compared to the case of isotropic spheres, due to the anisotropy of the tactoids and the individual layers that prevent free-rotation of these elements and, thus, dissipation of stress. The extent of percolation of the network can increase in two ways for PP nanocomposites [37]: one is by an increase in the number of stacks based on the assumption that layer thickness and size are the same (case I). The other is by an increase in the degree of exfoliation (case II). Case I would correspond to the increase of the amount of clay at a fixed PP-*g*-MA content while case II would correspond to the increase of PP-*g*-MA content at a fixed clay content.

Based on these points of view, we carried out frequency sweep tests for TPO nanocomposites with different amounts of clay and PP-*g*-MA at 180 °C. Fig. 21 shows the rheological properties for TPO nanocomposites with different amounts of

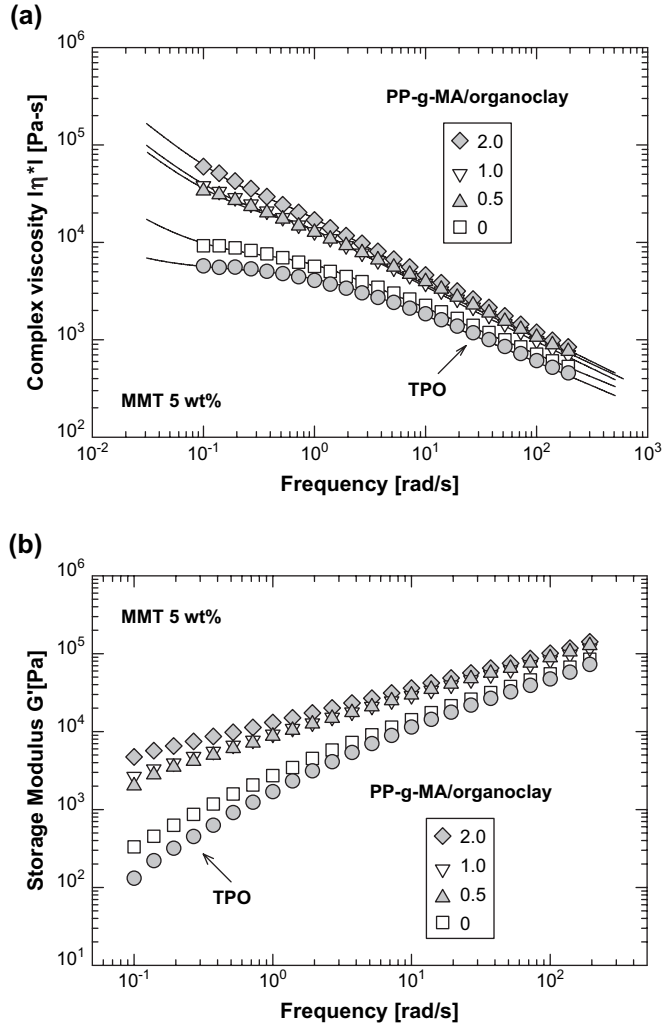

Fig. 22. Frequency sweep results for TPO nanocomposites at 180 °C. (a) Complex viscosity and (b) storage modulus for different ratios of PP-*g*-MA/organoclay at a fixed MMT of 5 wt%. Solid line indicates the empirical fitting of complex viscosity with Eq. (5).

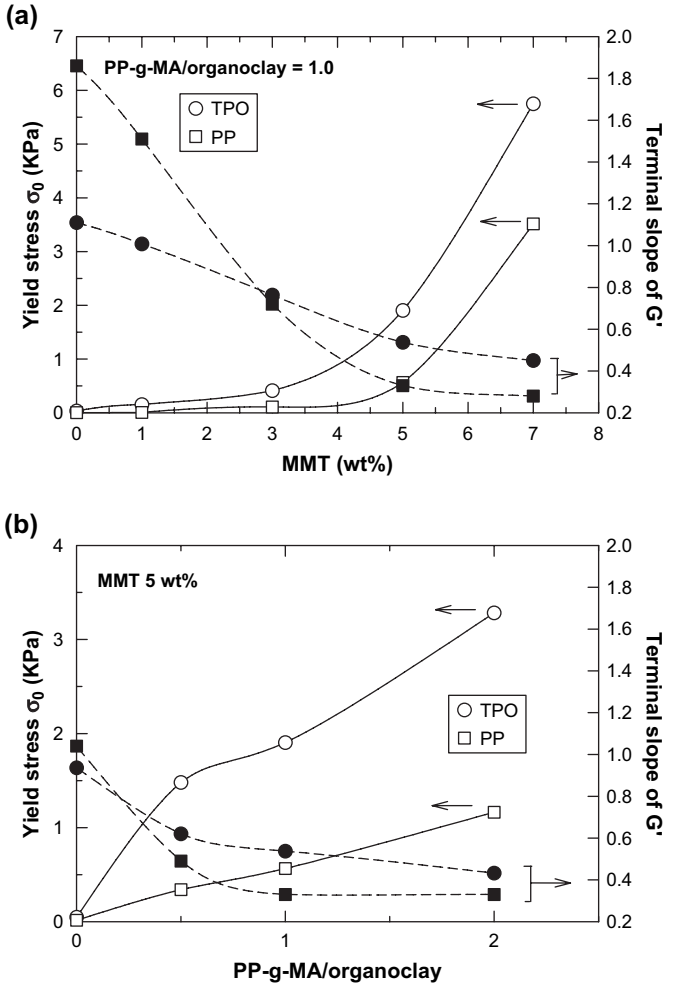

Fig. 23. Comparison of melt yield stress and terminal slope of storage modulus at 180 °C as a function of (a) MMT content and (b) PP-*g*-MA/organoclay ratio for TPO-based and PP-based nanocomposites. The yield stress and terminal slope for PP-based nanocomposites are calculated using the data in Ref. [37].

clay at a fixed ratio of PP-*g*-MA to organoclay of 1.0. The complex viscosity shows increased shear-thinning behavior. When compared with pure TPO, the moduli increase progressively and their slopes decrease at low frequencies as clay content increases. As mentioned above, this is attributed to the percolated network caused by the increased number of clay layers (case I). Fig. 22 shows the rheological properties for TPO nanocomposites at various PP-*g*-MA/organoclay ratios and a fixed MMT content of 5 wt%. Compared with pure TPO, the moduli also increase progressively and the slopes decrease at low frequencies as PP-*g*-MA content increases (Fig. 22(b)). As mentioned above, this is attributed to the percolated network caused by an increased degree of exfoliation (case II). We have reported similar rheological behavior for PP-based nanocomposites [37]. However, it is difficult to distinguish the effects of the elastomer phase on the rheological behavior from that of clay platelets. To address this issue quantitatively, a comparison of the yield stresses and terminal slopes of these materials is made below.

Lertwimolnun and Vergnes [32] proposed using a Carreau–Yasuda model with a melt yield stress to describe the melt rheology of PP-based nanocomposites, i.e.,

$$\eta(\omega) = \frac{\sigma_0}{\omega} + \eta_0[1 + (\lambda\omega)^a]^{(n-1)/a} \tag{5}$$

where σ_0 is the yield stress, ω is the angular frequency, η_0 is the zero shear viscosity, λ is the time constant, a is the Yasuda parameter and n is the dimensionless power law index. These five parameters were adjusted to obtain the best fit with the experimental data, see the solid lines in Figs. 21(a) and 22(a). For the current series of materials, the time constant λ changes from 0.8 to 4.0 s and the dimensionless power law index n changes from 0.4 to 0.6. The important parameter of yield stress is shown as a function of MMT content and PP-*g*-MA/organoclay ratio in Fig. 23. The yield stress increases as the MMT content and/or the PP-*g*-MA/organoclay ratio increases. For all compositions, the yield stress of TPO-based nanocomposites is larger than that of PP-based nanocomposites due to the presence of an elastic

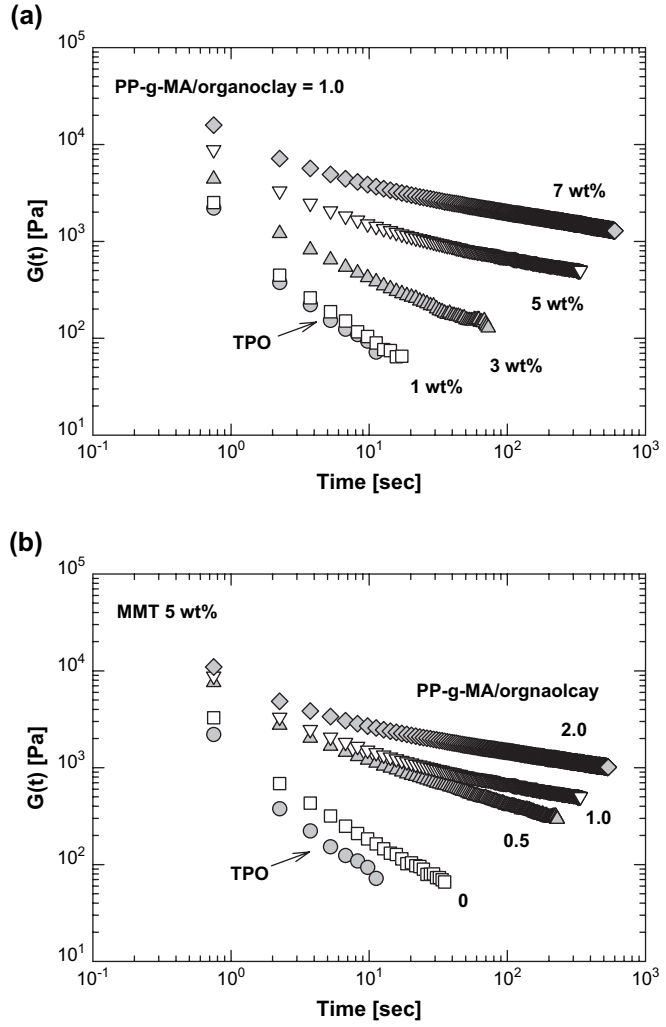

Fig. 24. Stress relaxation data for TPO nanocomposites. (a) Different MMT concentration at a fixed ratio of PP-*g*-MA/organoclay = 1.0 and (b) different ratio of PP-*g*-MA/organoclay at a fixed MMT concentration of 5.0 wt%.

rubber phase. On the other hand, the terminal slopes of G' for TPO and PP-based nanocomposites decrease as the MMT content and/or the PP-*g*-MA/organoclay ratios increase. The terminal slopes are calculated in the low frequency region below 1 rad/s. Without PP-*g*-MA or organoclay, the value of the terminal slope for TPO is lower than that of PP because TPO contains elastic rubber phase. However, the terminal slope for PP decreases sharply as MMT content increases; whereas, that for TPO decreases steadily and shows higher values than that of PP at higher MMT content and PP-*g*-MA/organoclay ratios. It is important to note that this tendency indicates that the elastomer phase in TPO suppresses the dispersion of organoclay. That is to say, the elastomer particles occupy volume in the matrix, resulting in a reduction of the volume affected by organoclay because of the poor affinity between the elastomer and the organoclay. This result is in good agreement with the morphological observation that the aspect ratio of organoclay in TPO decreases steadily while that in PP decreases sharply at low MMT content due to the presence of elastomer (see Fig. 9).

Fig. 24 shows stress relaxation results for TPO nanocomposites at 180 °C for different clay concentrations for a fixed PP-*g*-MA/organoclay of 1.0 (a) and for various ratios of PP-*g*-MA/organoclay for a fixed MMT content of 5 wt% (b). These results show that the relaxation time is dramatically increased as the amount of clay increases or as the ratio of PP-*g*-MA/organoclay increases. For any fixed time after the imposition of strain, the modulus is larger with higher clay loadings or higher PP-*g*-MA/organoclay ratios, similar to what was observed in the dynamic frequency test. At long times, the nanocomposites with low clay content appear to relax like a liquid while the nanocomposites with high MMT contents (>3 wt%) behave more like a solid. Based on both the dynamic oscillatory shear and the stress relaxation moduli, it is clear that the addition of clay particles or the increase of PP-*g*-MA/organoclay ratio has a profound influence on the stress relaxation of the TPO nanocomposites at long times [65].

4. Conclusion

The structure–property relationships of TPO/PP-*g*-MA/MMT nanocomposites prepared by melt processing have been investigated with a main focus on the ratio of PP-*g*-MA to organoclay. Morphological observations were used to interpret the mechanical and rheological properties of these nanocomposites. Detailed quantitative analyses of the dispersed clay particles and the elastomer phase revealed that the aspect ratio of clay particles decreased as the clay content increased, but it increased as the amount of PP-*g*-MA increased; whereas, the aspect ratio of the elastomer phase increased in both cases. The presence of clay causes the elastomer particles to become highly elongated in shape. The modulus and yield strength are enhanced by increasing the PP-*g*-MA/organoclay ratios. High levels of toughness of the TPO can be maintained when moderate levels of MMT and PP-*g*-MA are used. The rheological properties suggest that the extent of a percolation network is enhanced by increasing the number of clay stacks at a fixed ratio of PP-*g*-MA to organoclay and by increasing the degree of exfoliation at a fixed clay content. The addition of clay particles and PP-*g*-MA has a profound influence on the long time relaxation of the TPO nanocomposites. Based on these analyses, it is clear that it is important to optimize the ratio of PP-*g*-MA and organoclay to obtain the desired balance of mechanical properties and processing characteristics for TPO nanocomposites.

Acknowledgements

The authors thank General Motors for funding this work and the permission to publish it. The authors would like to thank Dr. Douglas Hunter, Dr. P.J. Yoon, and Mr. Tony Gonzales of Southern Clay Products for technical assistance and for providing materials. The authors also would like to thank Prof. Seung Jong Lee and Prof. Kyung Hyun Ahn of Seoul National University for rheological measurements.

References

[1] Giannelis EP. Adv Mater 1996;8(1):29–35.
[2] Alexandre M, Dubois P. Mater Sci Eng R Rep 2000;28(1–2):1–63.
[3] Collister J. In: Vaia RA, Krishnamoorti R, editors. Polymer nanocomposites: synthesis, characterization, and modeling. London: Oxford University Press; 2002 [chapter 2].
[4] Ray SS, Okamoto M. Prog Polym Sci 2003;28(11):1539–641.
[5] Hussain F, Hojjati M, Okamoto M, Gorga RE. J Compos Mater 2006;40(17):1511–75.
[6] Utracki LA, Sepehr M, Boccaleri E. Polym Adv Technol 2007;18(1):1–37.
[7] Lele A, Mackley M, Galgali G, Ramesh C. J Rheol 2002;46(5):1091–110.
[8] Liu X, Wu Q. Polymer 2001;42(25):10013–9.
[9] Marchant D, Jayaraman K. Ind Eng Chem Res 2002;41(25):6402–8.
[10] Nam PH, Maiti P, Okamoto M, Kotaka T, Hasegawa N, Usuki A. Polymer 2001;42(23):9633–40.
[11] Reichert P, Nitz H, Klinke S, Brandsch R, Thomann R, Mulhaupt R. Macromol Mater Eng 2000;275:8–17.
[12] Reichert P, Hoffmann B, Bock T, Thomann R, Mulhaupt R, Friedrich C. Macromol Rapid Commun 2001;22(7):519–23.
[13] Kodgire P, Kalgaonkar R, Hambir S, Bulakh N, Jog JP. J Appl Polym Sci 2001;81(7):1786–92.
[14] Zhang Q, Wang Y, Fu Q. J Polym Sci Part B Polym Phys 2003;41(1):1–10.
[15] Galgali G, Ramesh C, Lele A. Macromolecules 2001;34(4):852–8.
[16] Garces JM, Moll DJ, Bicerano J, Fibiger R, McLeod DG. Adv Mater 2000;12(23):1835–9.
[17] Hasegawa N, Okamoto H, Kawasumi M, Kato M, Tsukigase A, Usuki A. Macromol Mater Eng 2000;280/281:76–9.
[18] Ishida H, Campbell S, Blackwell J. Chem Mater 2000;12(5):1260–7.
[19] Garcia-Lopez D, Picazo O, Merino JC, Pastor JM. Eur Polym J 2003;39(5):945–50.
[20] Hasegawa N, Usuki A. J Appl Polym Sci 2004;93(1):464–70.
[21] Ellis TS, D'Angelo JS. J Appl Polym Sci 2003;90(6):1639–47.
[22] Jancar J, Dibenedetto AT. J Mater Sci 1994;29(17):4651–8.
[23] Jang BZ, Uhlmann DR, Vander Sande JB. J Appl Polym Sci 1985;30(6):2485–504.
[24] Long Y, Shanks RA. J Appl Polym Sci 1996;62(4):639–46.
[25] Ou Y-C, Guo T-T, Fang X-P, Yu Z-Z. J Appl Polym Sci 1999;74(10):2397–403.
[26] Li Y, Wei G-X, Sue H-J. J Mater Sci 2002;37(12):2447–59.
[27] Tjong SC, Meng YZ, Hay AS. Chem Mater 2002;14(1):44–51.
[28] Sun T, Garces JM. Adv Mater 2002;14(2):128–30.
[29] Kim DH, Park JU, Ahn KH, Lee SJ. Macromol Rapid Commun 2003;24(5–6):388–91.
[30] Kim DH, Cho KS, Mitsumata T, Ahn KH, Lee SJ. Polymer 2006;47(16):5938–45.
[31] Kim DH, Park JU, Cho KS, Ahn KH, Lee SJ. Macromol Mater Eng 2006;291(9):1127–35.
[32] Lertwimolnun W, Vergnes B. Polymer 2005;46(10):3462–71.
[33] Mehta S, Mirabella FM, Rufener K, Bafna A. J Appl Polym Sci 2004;92(2):928–36.
[34] Mishra JK, Hwang KJ, Ha CS. Polymer 2005;46(6):1995–2002.
[35] Lee H-s, Fasulo PD, Rodgers WR, Paul DR. Polymer 2005;46(25):11673–89.
[36] Lee H-s, Fasulo PD, Rodgers WR, Paul DR. Polymer 2006;47(10):3528–39.
[37] Kim DH, Fasulo PD, Rodgers WR, Paul DR. Polymer 2007;48(18):5308–23.
[38] Fornes TD, Yoon PJ, Keskkula H, Paul DR. Polymer 2001;42(25):9929–40.
[39] Fornes TD, Yoon PJ, Keskkula H, Paul DR. Polymer 2002;43(7):2121–2.
[40] Fornes TD, Hunter DL, Paul DR. Polymer 2004;45(7):2321–31.
[41] Yoon PJ, Fornes TD, Paul DR. Polymer 2002;43(25):6727–41.
[42] Chavarria F, Paul DR. Polymer 2004;45(25):8501–15.
[43] Chin IJ, Thurn-Albrecht T, Kim HC, Russell TP, Wang J. Polymer 2001;42(13):5947–52.
[44] Yalcin B, Cakmak M. Polymer 2004;45(19):6623–38.
[45] Piner RD, Xu TT, Fisher FT, Qiao Y, Ruoff RS. Langmuir 2003;19(19):7995–8001.
[46] Khatua BB, Lee DJ, Kim HY, Kim JK. Macromolecules 2004;37(7):2454–9.
[47] Gelfer MY, Song HH, Liu L, Hsiao BS, Chu B, Rafailovich M, et al. J Polym Sci Part B Polym Phys 2002;41(1):44–54.
[48] Si M, Araki T, Ade H, Kilcoyne ALD, Fisher R, Sokolov JC, et al. Macromolecules 2006;39(14):4793–801.
[49] Wang Y, Zhang Q, Fu Q. Macromol Rapid Commun 2003;24(3):231–5.
[50] Ray SS, Pouliot S, Bousmina M, Utracki LA. Polymer 2004;45(25):8403–13.
[51] Wang SF, Hu YA, Song L, Liu J, Chen ZY, Fan WC. J Appl Polym Sci 2004;91(3):1457–62.
[52] Hong JS, Namkung H, Ahn KH, Lee SJ, Kim C. Polymer 2006;47(11):3967–75.
[53] Chow WS, Ishak ZAM, Karger-Kocsis J, Apostolov AA, Ishiaku US. Polymer 2003;44(24):7427–40.
[54] Chow WS, Ishak ZAM, Ishiaku US, Karger-Kocsis J, Apostolov AA. J Appl Polym Sci 2004;91(1):175–89.
[55] Yoo Y, Park C, Lee SG, Choi KY, Kim DS, Lee JH. Macromol Chem Phys 2005;206(8):878–84.
[56] Wu S. Polymer 1985;26(12):1855–63.
[57] Liang JZ, Li RKY. J Appl Polym Sci 2000;77(2):409–17.
[58] Jiang W, Tjong SC, Li RKY. Polymer 2000;41(9):3479–82.
[59] Jiang W, Yu D, Jiang B. Polymer 2004;45(19):6427–30.
[60] Vermogen A, Masenelli-Varlot K, Seguela R, Duchet-Rumeau J, Boucard S, Prele P. Macromolecules 2005;38(23):9661–9.
[61] Morgan AB, Gilman JW. J Appl Polym Sci 2003;87(8):1329–38.
[62] Huang JJ, Keskkula H, Paul DR. Polymer 2006;47(2):639–51.
[63] Shah RK, Hunter DL, Paul DR. Polymer 2005;46(8):2646–62.
[64] Schmidt G, Nakatani AI, Butler PD, Karim A, Han CC. Macromolecules 2000;33(20):7219–22.
[65] Ren J, Silva AS, Krishnamoorti R. Macromolecules 2000;33(10):3739–46.
[66] Krishnamoorti R, Yurekli K. Curr Opin Colloid Interface Sci 2001;6(5,6):464–70.